Published in Comput. Methods Appl. Mech. Engrg. 233/236 (2012), 123–136.

Topological derivative-based topology optimization of structures subject to Drucker-Prager stress constraints

S. Amstutz

Laboratoire d'analyse non linéaire et géométrie, Faculté des Sciences, Université D'Avignon, 33 rue Louis Pasteur, 84000 Avignon, France.

A.A. Novotny

Laboratório Nacional de Computação Científica LNCC/MCT, Coordenação de Matemática Aplicada e Computacional, Av. Getúlio Vargas 333, 25651-075 Petrópolis - RJ, Brazil.

E.A. de Souza Neto*

Civil and Computational Engineering Centre, College of Engineering, Swansea University, Singleton Park, Swansea SA2 8PP, UK

Abstract

An algorithm for topology optimization of elastic structures under plane stress subject to the Drucker-Prager stress constraint is presented. The algorithm is based on the use of the topological derivative of the associated objective functional in conjunction with a level-set representation of the structure domain. In this context, a penalty functional is proposed to enforce the point-wise stress constraint and a closed formula for its topological derivative is derived. The resulting algorithm is of remarkably simple computational implementation. It does not require post-processing procedures of any kind and features only a minimal number of user-defined algorithmic parameters. This is in sharp contrast with current procedures for topological structural optimization with local stress constraints. The effectiveness and efficiency of the algorithm presented here are demonstrated by means of numerical exam-

*Corresponding author.

Email addresses: samuel.amstutz@univ-avignon.fr (S. Amstutz), novotny@lncc.br (A.A. Novotny), E.deSouzaNeto@swansea.ac.uk (E.A. de Souza Neto)

ples. The examples show, in particular, that it can easily handle structural optimization problems with underlying materials featuring strong asymmetry in their tensile and compressive yield strengths.

Keywords:
topological sensitivity, topological derivative, topology optimization, Drucker-Prager criterion, local stress constraint

1. Introduction

Over the last two decades or so, the development of algorithms for topology optimization of linear elastic load-bearing structures has attracted considerable attention in computational mechanics circles. As a result of the continuous research efforts in this direction a wide body of literature is currently available on this topic and various computational procedures are well established and can be applied to a range of practical problems of industrial interest [16, 1, 10]. Many such procedures, almost invariably used in conjunction with finite element methods of structural analysis, are even available in off-the-shelf commercial software packages (e.g. Altair® OptiStruct® [28] and Genesis® [19]).

To date, most developments in this field have relied on so-called *SIMP methods* (solid isotropic material with penalization), where the physical black-and-white topology of the optimal structure, i.e. a topology consisting of either material (black) or empty space (white) at each point of the computational domain, is approximated by means of a fictitious density field displaying a smooth (grey) transition in the otherwise black-white interface (the boundary of the structure domain). Such methods have been widely applied with success to problems such as compliance minimization [10] but, despite its fundamental importance in engineering design, only a relatively small number of publications appear to deal with the incorporation of local (point-wise) stress constraints [2, 3, 11, 14, 18, 22, 29]. This can be probably justified by the challenges resulting from the typically very large number of highly non-linear constraints involved as well as by the need for carefully designed stress relaxation procedures to address a side effect of the density field-based regularization of the original black-and-white problem [22].

More recently, a new class of methodologies for structural topology optimization has emerged based on the use of the *topological derivative* of the relevant objective functionals [31, 12, 26, 5, 25, 27]. The notion of topologi-

cal derivative itself is a relatively new concept, introduced just over a decade ago [12, 31]. Further theoretical developments are reported, among others, in [24, 4, 30]. An early application of this idea to topology compliance optimization, prior to its precise mathematical definition in a general context, is described in [17]. The topological derivative concept extends the conventional notion of derivative to functionals whose variable is a geometrical domain subject to singular topology changes. In structural topology optimization for instance, it gives the *exact* sensitivity of the associated objective functionals to black-and-white-type topological perturbations such as the insertion of infinitesinal holes or inclusions of different material properties. Crucial here is the fact that the topological derivative of the objective functional contains fundamental information that accurately indicates descent directions associated with exact black-and-white-type topology changes, without the need for black-grey-white-type regularisation procedures. In this context, a topological derivative-based algorithm with a level-set representation of the structure domain has been proposed in [5] and shown to efficiently solve compliance minimization problems. More recently, following the ideas presented in [6] for the Laplace equation, this algorithm has been further developed in [8] to incorporate local stress constraints of the von Mises type by means of a penalty approach in plane stress problems. One striking feature of the algorithm of [8] is its simplicity of implementation. Once a suitable penalized objective functional has been defined and a closed formula for its topological derivative obtained, the locally stress-constrained topology optimization problem is treated algorithmically in exactly the same way as its unconstrained counterpart. In particular, in contrast to current methods of stress-constrained topology optimization, the topological derivative-based procedure does not require post-processing (e.g. procedures such as density filtering, ε-relaxation [22]) of any kind and only a minimal number of user-defined algorithmic parameters (e.g. penalty coefficient) are needed. This relative algorithmic simplicity is nothing but a natural consequence of the use of the topological derivative in defining the descent direction, which is based on the exact black-and-white definition of the topology optimization problem. In fairness to other methods of topology optimization, however, we should note that the striking algorithmic simplicity here comes at the cost of derivation of a closed formula for the topological derivative of the objective functional which may prove to be a laborious mathematical task.

Our main purpose in this paper is to extend the work reported in [8] to incorporate point-wise stress constraints of the Drucker-Prager type [15]. In

particular, we want to minimize the volume of the structure domain requiring at the same time the stress tensor at each point of the loaded optimized structure to be bound by a Drucker-Prager-type yield criterion. In this context, a suitable penalty functional for the enforcement of the Drucker-Prager constraint is proposed and a closed formula for its topological derivative is obtained. We recall that the Drucker-Prager yield criterion was originally conceived as a smooth approximation to the classical Mohr-Coulomb criterion for soils and geomaterials (refer for instance to [13]). Under plane stress (the case considered here) it may be used as a general model for materials with distinct tensile and compressive yield strengths, such as concrete, masonry and wood. The overall optimization algorithm is described in detail and numerical examples are presented to demonstrate its effectiveness and efficiency in the treatment of structural optimization under the present stress constraints. In particular, unlike stress-unconstrained optimization, the results here show that the obtained optimized structures are free from geometrical singularities that result in (highly undesirable) stress concentration.

The paper is organized as follows. Section 2 states the stress-constrained topology optimization problem and defines the penalized version to be solved by the algorithm. Section 3 presents a closed formula for the topological derivative of the corresponding penalized objective functional. The optimization algorithm is described in Section 4 and its application in numerical examples is presented in Section 5. Concluding remarks are drawn in Section 6. The closed formula presented in Section 3 for the topological derivative of the proposed Drucker-Prager penalty functional is derived in detail in Appendix A.

2. The topology optimization problem

Our purpose here is to find optimal topologies for two-dimensional elastic structures under plane stress condition loaded by a given system of mechanical loads with prescribed kinematical boundary conditions and subject to a point-wise constraint on the stress tensor. More specifically, we want to minimize the volume of the structure domain requiring at the same time the stress tensor at each point of the loaded optimized structure to be bound by a Drucker-Prager-type yield criterion. The corresponding optimization problem is mathematically stated in the following.

2.1. The constrained optimization problem

Let $D \subset \Re^2$ be a bounded domain with Lipschitz boundary Γ defining the so-called *hold-all* domain (refer to Fig. 1). The domain of the sought optimal structure will be a subset of the hold-all domain. The boundary Γ is the union of three given non-overlapping subsets, Γ_D, Γ_N and Γ_0. Displacements are prescribed on Γ_D and non-zero and zero boundary tractions are prescribed respectively on Γ_N and Γ_0. In addition, we conveniently assume that the stress constraint is to be enforced on a given open subset $\widetilde{D}$ of D. Note that stress constraints cannot usually be enforced, for instance, in the surroundings of point supports or point loads and, hence, $\widetilde{D} \neq D$ in general.

Given a hold-all domain D and a stress constraint-enforcement subdomain $\widetilde{D}$, the optimisation problem consists in finding a subdomain $\Omega \subset D$ (the optimal structure domain) that solves the following constrained minimization problem:

$$\underset{\Omega \subset D}{\text{Minimize}}\, I_\Omega(\boldsymbol{u}_\Omega), \tag{1}$$

with I_Ω the *objective functional*

$$I_\Omega(\boldsymbol{u}_\Omega) := |\Omega| + \beta K_\Omega(\boldsymbol{u}_\Omega); \qquad K_\Omega(\boldsymbol{u}_\Omega) := \int_{\Gamma_N} \boldsymbol{g} \cdot \boldsymbol{u}_\Omega \, ds, \tag{2}$$

subject to the elastic equilibrium equations,

$$\left\{ \begin{array}{rcll} \mathrm{div}\boldsymbol{\Sigma}(\boldsymbol{u}_\Omega) &=& 0 \quad \text{in} \quad D \\ \boldsymbol{u}_\Omega &=& 0 \quad \text{on} \quad \Gamma_D \\ \boldsymbol{\Sigma}(\boldsymbol{u}_\Omega)\boldsymbol{n} &=& \boldsymbol{g} \quad \text{on} \quad \Gamma_N \\ \boldsymbol{\Sigma}(\boldsymbol{u}_\Omega)\boldsymbol{n} &=& 0 \quad \text{on} \quad \Gamma_0, \end{array} \right. \tag{3}$$

and a point-wise Drucker-Prager constraint on the stress tensor $\boldsymbol{\Sigma}$:

$$\Sigma_M(\boldsymbol{u}_\Omega) + \eta \, \mathrm{tr}\boldsymbol{\Sigma}(\boldsymbol{u}_\Omega) \leq \overline{\sigma}^\star \qquad \text{a.e. in } \Omega \cap \widetilde{D}, \tag{4}$$

with Σ_M the von Mises effective stress:

$$\Sigma_M := \sqrt{\tfrac{3}{2}\boldsymbol{\Sigma}_d \cdot \boldsymbol{\Sigma}_d}, \tag{5}$$

and $\boldsymbol{\Sigma}_d$ the stress deviator. The given scalar constants η and $\overline{\sigma}^\star$ in (4) are the Drucker-Prager yield criterion parameters [15, 13] associated, respectively, with the Drucker-Prager cone angle and cohesion intersect. In (2,3), $\boldsymbol{g}$ is the

prescribed boundary traction field on the given portion Γ_N of the boundary and is assumed to belong to $L^2(\Gamma_N)^2$, $\boldsymbol{n}$ in (3) is the outward unit normal vector field on Γ and $\boldsymbol{u}_\Omega$ is the *displacement field* that solves the elastic equilibrium equations. The objective functional defined in (2) is well-suited for the minimization of the volume $|\Omega|$ of the structure subject to a pointwise stress constraint and has been used in [8] in conjunction with a von Mises stress constraint. The parameter $\beta > 0$ multiplying the compliance integral on the right hand side of (2) regularises the stress-constrained volume minimization problem which is otherwise ill-posed.

The subscript Ω is used here to emphasise that the relevant quantities (e.g. I_Ω, $\boldsymbol{u}_\Omega$) depend on the domain Ω – the design variable of problem (1). Throughout the paper, we assume (3) to hold in the weak sense and its solution,

$$\boldsymbol{u}_\Omega \in \mathcal{V} = \{\boldsymbol{u} \in H^1(D)^2, \boldsymbol{u}_{|\Gamma_D} = 0\}, \tag{6}$$

to be unique. The space $\mathcal{V}$ is the corresponding space of kinematicaly admissible displacement fields. The notation $\boldsymbol{\Sigma}(\boldsymbol{u}_\Omega)$ is used to emphasize that the stress tensor is a functional of the displacement field $\boldsymbol{u}_\Omega$ through the linear elastic constitutive equation:

$$\boldsymbol{\Sigma}(\boldsymbol{u}) = \mathbb{C}\,\boldsymbol{e}(\boldsymbol{u}), \tag{7}$$

where $\boldsymbol{e}$ is the infinitesimal strain tensor,

$$\boldsymbol{e}(\boldsymbol{u}) = \tfrac{1}{2}(\nabla \boldsymbol{u} + \nabla \boldsymbol{u}^T), \tag{8}$$

and

$$\mathbb{C} = 2\mu_\Omega \mathbb{I} + \lambda_\Omega (\boldsymbol{I} \otimes \boldsymbol{I}), \tag{9}$$

with μ_Ω and λ_Ω denoting the Lamé coefficients and $\mathbb{I}$ and $\boldsymbol{I}$ the fourth- and second-order identity tensors respectively. The statement of the minimization problem is completed with the definition of a piece-wise constant Young's modulus field over D as follows:

$$E_\Omega = \begin{cases} E_{\text{hard}} & \text{in} \quad \Omega \\ E_{\text{soft}} & \text{in} \quad D \setminus \overline{\Omega}, \end{cases} \tag{10}$$

with

$$E_{\text{soft}} \ll E_{\text{hard}}. \tag{11}$$

That is, the original optimization problem, where the structure itself consists of the domain Ω of given elastic properties and the remaining part $D \setminus \overline{\Omega}$

of the hold-all is empty (has no material), is approximated by means of the two-phase material distribution (10) over D where the empty region $D \setminus \overline{\Omega}$ is occupied by a material (the soft phase) with Young's modulus, E_{soft}, much lower than the given Young's modulus E_{hard} of the structure material (the hard phase). Both phases share the same Poisson's ratio ν. The corresponding Lamé coefficients under plane stress read

$$\mu_\Omega = \frac{E_\Omega}{2(1+\nu)}, \qquad \text{and} \qquad \lambda_\Omega = \frac{\nu E_\Omega}{1-\nu^2}. \tag{12}$$

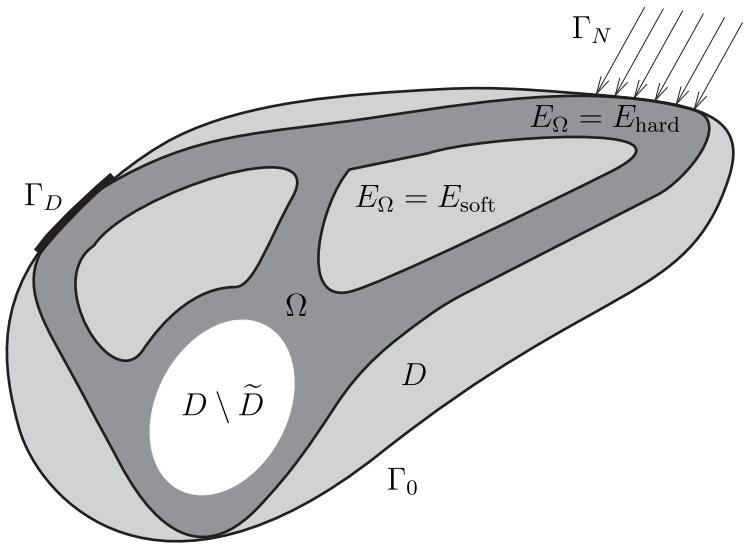

Figure 1: Sketch of the hold-all domain.

2.2. The penalized optimization problem

The presence of the point-wise stress constraint (4) makes it difficult to treat the above constrained optimization problem directly. This issue has been recently discussed in some detail by Le *et al.* [22] in the context of SIMP methods for structural optimization [10]. To tackle the problem here we follow a radically different approach proposed in [8]. It relies on a topological derivative-based algorithm in conjunction with an approximation of the original constrained problem by means of a penalty regularization of the point-wise stress constraint. The penalized problem is obtained in the following.

Before defining the corresponding penalty functional it is convenient in the present case to re-phrase the stress constraint (4) in terms of normalized quantities. To this end we define the *normalized stress tensor*:

$$\boldsymbol{\sigma} := \boldsymbol{\Sigma}/E_\Omega, \tag{13}$$

and the *normalized cohesion intersect-related parameter* of the Drucker-Prager yield surface:

$$\overline{\sigma} := \overline{\sigma}^\star/E_\Omega. \tag{14}$$

By rewriting (4) as

$$\Sigma_M(\boldsymbol{u}_\Omega) \leq \overline{\sigma}^\star - \eta\,\mathrm{tr}\boldsymbol{\Sigma}(\boldsymbol{u}_\Omega), \tag{15}$$

squaring both sides and making use of the above definitions, we obtain after a straightforward manipulation an equivalent statement of the Drucker-Prager stress constraint in terms of normalized stresses:

$$\Upsilon(\boldsymbol{\sigma}(\boldsymbol{u})) := \tfrac{1}{2}\widetilde{\mathbb{B}}\boldsymbol{\sigma}(\boldsymbol{u})\cdot\boldsymbol{\sigma}(\boldsymbol{u}) + 2\eta\overline{\sigma}\,\mathrm{tr}\boldsymbol{\sigma}(\boldsymbol{u}) \leq \overline{\sigma}^2, \tag{16}$$

where

$$\widetilde{\mathbb{B}} = 3\mathbb{I} - (1+2\eta^2)\boldsymbol{I}\otimes\boldsymbol{I}. \tag{17}$$

Alternatively, by taking the elastic law (7,9) into account, (16) can be expressed as

$$\tfrac{1}{2}\mathbb{B}\boldsymbol{\sigma}(\boldsymbol{u})\cdot\boldsymbol{e}(\boldsymbol{u}) + \xi\,\mathrm{tr}\boldsymbol{e}(\boldsymbol{u}) \leq \overline{\sigma}^2, \tag{18}$$

where

$$\mathbb{B} = 6\mu\mathbb{I} + \lambda(1-4\eta^2)(\boldsymbol{I}\otimes\boldsymbol{I}) - 2\mu(1+2\eta^2)(\boldsymbol{I}\otimes\boldsymbol{I}) \tag{19}$$

with μ and λ the normalized Lamé coefficients:

$$\mu := \frac{\mu_\Omega}{E_\Omega}; \qquad \lambda := \frac{\lambda_\Omega}{E_\Omega} \tag{20}$$

and

$$\xi := 4(\mu+\lambda)\eta\overline{\sigma}. \tag{21}$$

With the above at hand, we now proceed to define the penalized objective function. Then, let $\Phi : \Re_+ \to \Re_+$ be a nondecreasing function of class $\mathcal{C}^2$. To allow a proper justification in the analysis presented in the appendix, we further assume that the derivatives Φ' and Φ'' are bounded. The *penalty functional* is defined as

$$J_\Omega(\boldsymbol{u}) := \int_{\widetilde{D}} E_\Omega\Phi(\Upsilon(\boldsymbol{\sigma}(\boldsymbol{u})))d\boldsymbol{x}. \tag{22}$$

According to (4), in the original optimization problem the stress is constrained in $\Omega \cap \tilde{D}$ – the portion of the elastic structure subject to the stress constraint. In the penalized version (22) – where a soft phase has been introduced to mimic the void region – the constraint must be imposed over the entire $\tilde{D}$. With the above penalty function, we define a corresponding *penalized objective functional* as

$$I_\Omega^\alpha(\boldsymbol{u}) := I_\Omega(\boldsymbol{u}) + \alpha J_\Omega(\boldsymbol{u}), \tag{23}$$

where the scalar $\alpha > 0$ is a given *penalty coefficient*. The original constrained optimization problem (1)-(4) with point-wise constraints can then be approximated by the following *penalized optimization problem*:

$$\underset{\Omega \subset D}{\text{Minimize}}\, I_\Omega^\alpha(\boldsymbol{u}_\Omega) \qquad \text{subject to (3).} \tag{24}$$

Problem (24) provides a good approximation to (1)-(4) so long as

(a) the penalty coefficient α is sufficiently large; and

(b) a function Φ is chosen such that Φ' varies sufficiently sharply around $\Upsilon(\boldsymbol{\sigma}(\boldsymbol{u})) = \overline{\sigma}^2$.

In particular, in the present paper we shall adopt a function Φ of the following functional format:

$$\Phi(t) \equiv \Phi_p(t), \tag{25}$$

where $p \geq 1$ is a given real parameter and $\Phi_p : \Re_+ \to \Re_+$ is defined as

$$\Phi_p(t) = \left[1 + \left(\tfrac{t}{\overline{\sigma}^2}\right)^p\right]^{1/p} - 1. \tag{26}$$

With this choice, the penalized problem (24) to be solved here reads explicitly

$$\underset{\Omega \subset D}{\text{Minimize}}\, I_\Omega^\alpha(\boldsymbol{u}_\Omega) = |\Omega| + \beta \int_{\Gamma_N} \boldsymbol{g}\cdot\boldsymbol{u}_\Omega \, ds + \alpha \int_{\widetilde{D}} E_\Omega \, \Phi_p(\Upsilon(\boldsymbol{\sigma}(\boldsymbol{u}_\Omega))) \, d\boldsymbol{x} \qquad \text{subject to (3).} \tag{27}$$

Remark 1. *Figure 2 shows the graph of function Φ_p for different values of p. Note that increasing values of p make Φ_p vary more sharply around $\Phi_p(\Upsilon(\boldsymbol{\sigma}(\boldsymbol{u}))) = 1$, i.e. around $\Upsilon(\boldsymbol{\sigma}(\boldsymbol{u})) = \overline{\sigma}^2$ (the Drucker-Prager cone in stress space) so that the requirement of item (b) above is met by this choice of Φ_p if p is sufficiently large. For increasing values of p and α, the penalizing term of (27) tends to a non-differentiable penalty functional, whose value is zero if the stress tensor is bound by the Drucker-Prager cone almost everywhere in $\widetilde{D}$ and ∞ otherwise.*

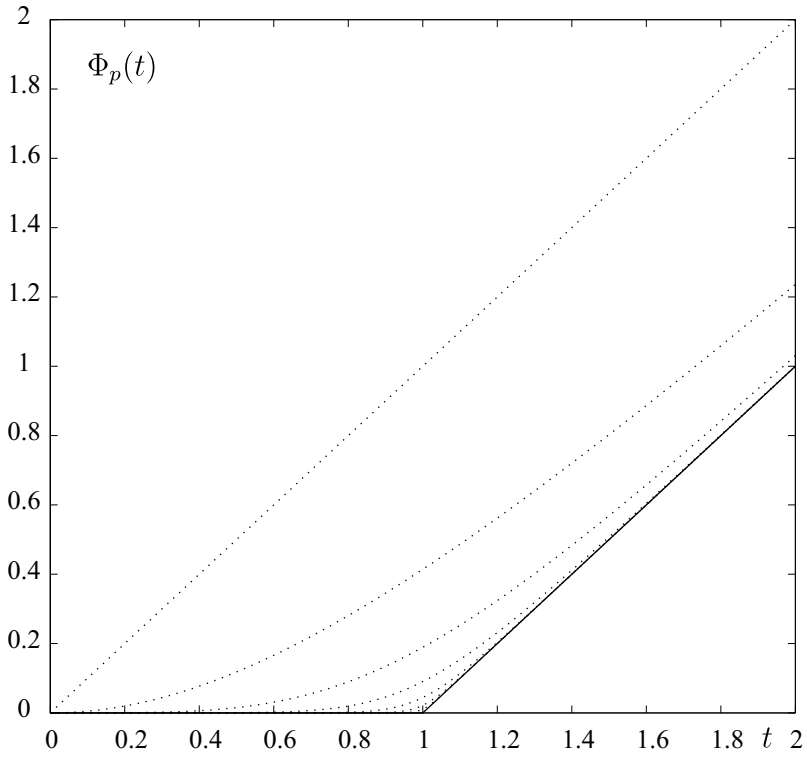

Figure 2: Function Φ_p with $\overline{\sigma} = 1$ for $p = 2^n$, $n = 0, ..., 6$.

3. Topological derivatives

The unconstrained minimization problem (27) will be solved in this paper by the algorithm described in Section 4, which relies fundamentally on the concept of *topological derivative*. This section provides a closed formula for the topological derivative of the penalized objective functional of (27) to be used in the algorithm. Before presenting the closed formula itself, a brief discussion on the relatively recent concept of topological derivative appears to be convenient and should be helpful to those not yet familiar with the idea.

3.1. The topological derivative concept

The notion of topological derivative extends the conventional definition of derivative to functionals whose variable is a *geometrical domain* subjected to singular topology changes. The idea can be introduced by considering a generic functional $G(\Omega)$ of a given domain Ω and assuming that Ω is subject

to topology changes consisting, say, of the introduction of a circular hole of radius ε centered at an arbitrary point $\widehat{\boldsymbol{x}} \in \Omega$. The resulting topologically changed domain, denoted $\Omega_\varepsilon(\widehat{\boldsymbol{x}})$, is the set defined as (refer to Fig. 3)

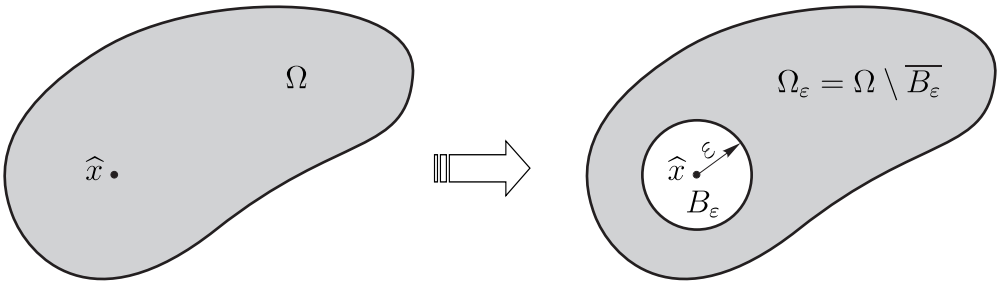

Figure 3: An example of topological domain perturbation.

$$\Omega_\varepsilon(\widehat{\boldsymbol{x}}) = \Omega \setminus \overline{B_\varepsilon(\widehat{\boldsymbol{x}})}, \tag{28}$$

where $\overline{B_\varepsilon(\widehat{\boldsymbol{x}})}$ denotes the closure of the domain of the inserted hole. The topological derivative of the functional G exists if its value $G(\Omega_\varepsilon)$ for the topologically perturbed domain Ω_ε can be expressed as a sum

$$G(\Omega_\varepsilon(\widehat{\boldsymbol{x}})) = G(\Omega) + f(\varepsilon)\, D_T G(\widehat{\boldsymbol{x}}) + o(f(\varepsilon)), \tag{29}$$

of the functional $G(\Omega)$ evaluated for the original domain Ω, a term $f(\varepsilon)\, D_T G(\widehat{\boldsymbol{x}})$ that varies linearly with a function $f(\varepsilon)$ and a remainder of the form $o(f(\varepsilon))$. The function $f : \Re_+ \to \Re_+$ must be such that $f(\varepsilon) \to 0$ when $\varepsilon \to 0_+$ and the remainder $o(f(\varepsilon))$ vanishes faster than $f(\varepsilon)$, with respect to ε, namely:

$$\lim_{\varepsilon \to 0} \frac{o(f(\varepsilon))}{f(\varepsilon)} = 0. \tag{30}$$

The right hand side of (29) is named the *topological asymptotic expansion* of G and the field $D_T G : \Omega \to \Re$ is the *topological derivative* of the functional G evaluated at the original domain Ω for the considered type of topological perturbation (the introduction of a circular hole). The topological derivative $D_T G$ itself can be expressed as

$$D_T G = \lim_{\varepsilon \to 0_+} \frac{G(\Omega_\varepsilon) - G(\Omega)}{f(\varepsilon)}. \tag{31}$$

The analogy between (29,31) and the corresponding expressions for a conventional derivative should be noted.

To illustrate the application of this concept, let us consider the (very simple) functional

$$G(\Omega) := |\Omega| = \int_{\Omega} d\boldsymbol{x}, \tag{32}$$

with Ω subject to the class of topological perturbations referred to in the above (circular holes). For two-dimensional domains Ω, the functional $G(\Omega)$ represents the area of the domain. The expansion (29) in this case can be obtained trivially as

$$\begin{aligned} G(\Omega_\varepsilon) \;=\; |\Omega_\varepsilon| \;&=\; \int_{\Omega} d\boldsymbol{x} - \int_{B_\varepsilon} d\boldsymbol{x} \\ &=\; G(\Omega) - \pi\varepsilon^2, \end{aligned} \tag{33}$$

and the topological derivative $D_T G$ and function f promptly identified as

$$D_T G = -\pi; \qquad f(\varepsilon) = \varepsilon^2. \tag{34}$$

In this particular case, $D_T G$ is independent of $\widehat{\boldsymbol{x}}$ and the rightmost term of the topological asymptotic expansion (29) is identically zero.

3.2. The topological derivative of the penalized objective functional

In the minimization problem (27) the hold-all domain is split as the union of a subset Ω occupied by the hard phase and its complement $D \setminus \overline{\Omega}$ occupied by the soft phase. In this case, it is appropriate to consider topological perturbations consisting of the introduction a circular inclusion of domain $B_\varepsilon(\widehat{\boldsymbol{x}})$ made of hard phase material if the perturbation point $\widehat{\boldsymbol{x}}$ lies in the soft phase domain and made of soft phase material if $\widehat{\boldsymbol{x}}$ lies in the hard phase domain. The corresponding perturbed structural domain $\Omega_\varepsilon(\widehat{\boldsymbol{x}})$, i.e. the domain of the hard phase after the introduction of the inclusion, reads

$$\Omega_\varepsilon(\widehat{\boldsymbol{x}}) = \begin{cases} \Omega \setminus \overline{B_\varepsilon(\widehat{\boldsymbol{x}})} & \text{if} \quad \widehat{\boldsymbol{x}} \in \Omega, \\ (\Omega \cup B_\varepsilon(\widehat{\boldsymbol{x}})) \cap D & \text{if} \quad \widehat{\boldsymbol{x}} \in D \setminus \overline{\Omega}. \end{cases} \tag{35}$$

The topological derivative of the unconstrained objective functional (27) is given by the sum

$$D_T I_\Omega^\alpha = D_T|\Omega| + \beta\, D_T K_\Omega + \alpha\, D_T J_\Omega, \tag{36}$$

of topological derivatives of each term on the right hand side of (27) with respect to the class of topological perturbations defined by (35). The first term $D_T|\Omega|$ above is trivial. Its derivation is completely analogous to that of the topological derivative $(34)_1$ of the same functional, $|\Omega|$, for topological perturbations in the form of introduction of circular holes. Here we have

$$D_T|\Omega| = \begin{cases} -\pi & \text{in } \Omega, \\ \pi & \text{in } D \setminus \overline{\Omega}. \end{cases} \tag{37}$$

The topological derivative $D_T K_\Omega$ of the compliance functional is known. It has been used in the context of structural optimization with topological derivative-based algorithms (refer, for instance, to [4, 20] for a detailed derivation). Its closed formula is

$$D_T K_\Omega = \pi(E_1 - E_0)(\rho\mathbb{T} - \mathbb{I})\boldsymbol{\sigma}(\boldsymbol{u}_\Omega) \cdot \boldsymbol{e}(\boldsymbol{u}_\Omega), \tag{38}$$

where

$$E_0(\widehat{\boldsymbol{x}}) = \begin{cases} E_{\text{hard}} & \text{if} \quad \widehat{\boldsymbol{x}} \in \Omega \\ E_{\text{soft}} & \text{if} \quad \widehat{\boldsymbol{x}} \in D \setminus \overline{\Omega}; \end{cases} \qquad E_1(\widehat{\boldsymbol{x}}) = \begin{cases} E_{\text{soft}} & \text{if} \quad \widehat{\boldsymbol{x}} \in \Omega \\ E_{\text{hard}} & \text{if} \quad \widehat{\boldsymbol{x}} \in D \setminus \overline{\Omega}, \end{cases} \tag{39}$$

the scalar ρ is

$$\rho = \frac{E_1 - E_0}{bE_1 + E_0}, \tag{40}$$

the fourth-order tensor $\mathbb{T}$ is the *polarization tensor* given by

$$\mathbb{T} = b\,\mathbb{I} + \frac{a - b}{2(1 + \gamma a)}\boldsymbol{I} \otimes \boldsymbol{I}, \tag{41}$$

with γ the elastic modulus contrast

$$\gamma = \frac{E_1}{E_0}, \tag{42}$$

and the constants a and b given by

$$a = \frac{1 + \nu}{1 - \nu}; \qquad b = \frac{3 - \nu}{1 + \nu}. \tag{43}$$

The derivation of the topological derivative $D_T J_\Omega$ of the penalty functional (22) for the Drucker-Prager stress constraint is rather involved. For the sake

of clarity we limit ourselves to presenting only the final formula here and leave its detailed derivation confined to Appendix A. The closed formula for $D_T J_\Omega$ reads

$$D_T J_\Omega = -\pi(E_1-E_0)\{\rho k_1(\boldsymbol{u}_\Omega)\mathbb{T}[\mathbb{B}\boldsymbol{\sigma}(\boldsymbol{u}_\Omega)+\xi\boldsymbol{I}]\cdot\boldsymbol{e}(\boldsymbol{u}_\Omega)+(\rho\mathbb{T}-\mathbb{I})\boldsymbol{\sigma}(\boldsymbol{u}_\Omega)\cdot\boldsymbol{e}(\boldsymbol{v}_\Omega)\}+ \pi E_1\chi_{\widetilde{D}}\{\Phi(\zeta_1(\boldsymbol{u}_\Omega)) + \rho k_1(\boldsymbol{u}_\Omega)\,[\widetilde{\mathbb{B}}\boldsymbol{\sigma}(\boldsymbol{u}_\Omega)\cdot\mathbb{T}\boldsymbol{\sigma}(\boldsymbol{u}_\Omega) + 2\eta\overline{\sigma}\,\mathrm{tr}(\mathbb{T}\boldsymbol{\sigma}(\boldsymbol{u}_\Omega))]\}+ E_0\chi_{\widetilde{D}}\{\Psi_\rho(\boldsymbol{\sigma}(\boldsymbol{u}_\Omega)) + \tfrac{1}{4}\pi\rho^2 k_1(\boldsymbol{u}_\Omega)\zeta_2(\boldsymbol{u}_\Omega)\} - \pi\chi_{\widetilde{D}}E_0\Phi(\Upsilon(\boldsymbol{\sigma}(\boldsymbol{u}_\Omega))), \quad (44)$$

where

$$k_1(\boldsymbol{u}_\Omega) = \chi_{\widetilde{D}}\,\Phi'(\Upsilon(\boldsymbol{\sigma}(\boldsymbol{u}_\Omega))), \quad (45)$$

with $\chi_{\widetilde{D}}$ the characteristic function of $\widetilde{D}$:

$$\chi_{\widetilde{D}}(\boldsymbol{x}) = \begin{cases} 1 & \text{if } \boldsymbol{x}\in\widetilde{D} \\ 0 & \text{otherwise.} \end{cases} \quad (46)$$

The functions ζ_1, ζ_2 and Ψ_ρ are given by

$$\zeta_1(\boldsymbol{u}_\Omega) = \Upsilon(\boldsymbol{\sigma}(\boldsymbol{u}_\Omega)) - \rho[\widetilde{\mathbb{B}}\boldsymbol{\sigma}(\boldsymbol{u}_\Omega)\cdot\mathbb{T}\boldsymbol{\sigma}(\boldsymbol{u}_\Omega) + 2\eta\overline{\sigma}\,\mathrm{tr}(\mathbb{T}\boldsymbol{\sigma}(\boldsymbol{u}_\Omega))]+ \rho^2\tfrac{1}{2}\widetilde{\mathbb{B}}\mathbb{T}\boldsymbol{\sigma}(\boldsymbol{u}_\Omega)\cdot\mathbb{T}\boldsymbol{\sigma}(\boldsymbol{u}_\Omega), \quad (47)$$

$$\zeta_2(\boldsymbol{u}_\Omega) = (5-8\eta^2)[2\boldsymbol{\sigma}(\boldsymbol{u}_\Omega)\cdot\boldsymbol{\sigma}(\boldsymbol{u}_\Omega) - \mathrm{tr}^2\boldsymbol{\sigma}(\boldsymbol{u}_\Omega)] + 3\Big(\tfrac{1+b\gamma}{1+a\gamma}\Big)^2\mathrm{tr}^2\boldsymbol{\sigma}(\boldsymbol{u}_\Omega), \quad (48)$$

and

$$\Psi_\rho(\boldsymbol{\sigma}(\boldsymbol{u}_\Omega)) = \int_0^1\int_0^\pi \frac{1}{t^2}[\Phi(\Upsilon(\boldsymbol{\sigma}(\boldsymbol{u}_\Omega)) + \Delta(t,\theta)) - \Phi(\Upsilon(\boldsymbol{\sigma}(\boldsymbol{u}_\Omega))) - \Phi'(\Upsilon(\boldsymbol{\sigma}(\boldsymbol{u}_\Omega)))\Delta(t,\theta)]\,d\theta\,dt, \quad (49)$$

with

$$\Delta(t,\theta) := \rho\tfrac{t}{2}\Big\{(\sigma_I-\sigma_{I\!I})\Big[(\sigma_I+\sigma_{I\!I})\Big(2(1-4\eta^2)+3\tfrac{1+b\gamma}{1+a\gamma}\Big)+8\eta\overline{\sigma}\Big]\cos\theta + 3(\sigma_I-\sigma_{I\!I})^2(2-3t)\cos 2\theta\Big\} + \big(\rho\tfrac{t}{2}\big)^2\Big\{3(\sigma_I+\sigma_{I\!I})^2\Big(\tfrac{1+b\gamma}{1+a\gamma}\Big)^2 + (\sigma_I-\sigma_{I\!I})^2\,(3(2-3t)^2+4(1-4\eta^2)\cos^2\theta) + 6\tfrac{1+b\gamma}{1+a\gamma}(\sigma_I^2-\sigma_{I\!I}^2)(2-3t)\cos\theta\Big\}, \quad (50)$$

where σ_I and σ_{II} are the eigenvalues of $\boldsymbol{\sigma}(\boldsymbol{u}_\Omega)$. The vector field $\boldsymbol{v}_\Omega$ in (44) is the solution of the adjoint equation

$$\left\{\begin{array}{rcll} -\text{div }\boldsymbol{\Sigma}(\boldsymbol{v}_\Omega) & = & +\text{div}[E_\Omega k_1(\boldsymbol{u}_\Omega)(\mathbb{B}\boldsymbol{\sigma}(\boldsymbol{u}_\Omega)+\xi\boldsymbol{I})] & \text{in} \quad D, \\ \boldsymbol{v}_\Omega & = & 0 & \text{on} \quad \Gamma_D, \\ \boldsymbol{\Sigma}(\boldsymbol{v}_\Omega)\,\boldsymbol{n} & = & -E_\Omega k_1(\boldsymbol{u}_\Omega)[\mathbb{B}\boldsymbol{\sigma}(\boldsymbol{u}_\Omega)+\xi\boldsymbol{I}]\,\boldsymbol{n} & \text{on} \quad \Gamma_N \cup \Gamma_0. \end{array}\right. \tag{51}$$

Formula (44) is valid for all $\widehat{\boldsymbol{x}} \in D \setminus \partial\widetilde{D} \setminus \partial\Omega$.

4. The topology design/optimization algorithm

The numerical solution of the penalized minimization problem (27) is undertaken here by the algorithm proposed in [5] in conjunction with a finite element approximation of the elastic boundary value problem (3) and the adjoint equation (51). The algorithm relies essentially on an optimality criterion based on the topological derivative of the objective function and on a level-set representation of the structure domain. It was proven very successful in the context of unconstrained structural optimization and optimization in problems of flow through porous media [5], in structural optimization under a von Mises stress constraint [8] and in the topology optimization of elastic microstructures [7].

With the level-set representation, the current structure domain Ω is characterized by a level-set function $\psi \in L^2(D)$ as

$$\Omega = \{\boldsymbol{x} \in D : \psi(\boldsymbol{x}) < 0\}, \tag{52}$$

and its complement as

$$D \setminus \overline{\Omega} = \{\boldsymbol{x} \in D : \psi(\boldsymbol{x}) > 0\}. \tag{53}$$

4.1. Topological derivative-based local optimality condition

The establishment of a local optimality condition based on the topological derivative field is straightforward. Indeed, note that for any given structure domain Ω, a negative (positive) value of the topological derivative $D_T I^\alpha_\Omega(\boldsymbol{x})$ at an arbitrary point $\boldsymbol{x} \in D$ indicates that the introduction of an infinitesimal circular inclusion centered at that point produces a perturbed domain whose objective functional value is smaller (greater) than that of the original

domain. From this observation we have that a sufficient condition of local optimality under the considered class of topological perturbations is that

$$D_T I_\Omega^\alpha(\boldsymbol{x}) > 0 \quad \forall\, \boldsymbol{x} \in D. \tag{54}$$

That is, (54) implies in the present context that the introduction of an infinitesimal circular inclusion at any point of D can only cause an increase in the value of the objective functional and, hence, Ω is indeed a locally optimum structure domain.

The algorithm described below is based on an alternative sufficient condition of local optimality, particularly convenient for use in conjunction with the level-set representation of the structure domain. The alternative condition can be established by first defining the scalar function,

$$g(\boldsymbol{x}) := \begin{cases} -D_T I_\Omega^\alpha(\boldsymbol{x}) & \text{if } \psi(\boldsymbol{x}) < 0 \\ \quad D_T I_\Omega^\alpha(\boldsymbol{x}) & \text{if } \psi(\boldsymbol{x}) > 0, \end{cases} \tag{55}$$

and then observing that, exclusively in terms of the function g and the level-set ψ, condition (54) is equivalent to

$$\begin{cases} g(\boldsymbol{x}) < 0 \;\text{ if }\; \psi(\boldsymbol{x}) < 0 \\ g(\boldsymbol{x}) > 0 \;\text{ if }\; \psi(\boldsymbol{x}) > 0. \end{cases} \tag{56}$$

Now, we note that (56) holds if the function g is a strictly positive scalar multiple of ψ, i.e.

$$\exists\, \tau > 0 \quad \text{s.t.} \quad g = \tau\, \psi, \tag{57}$$

or, equivalently,

$$\theta := \arccos\left[\frac{\langle g, \psi\rangle}{\|g\|_{L^2(D)}\, \|\psi\|_{L^2(D)}}\right] = 0, \tag{58}$$

where θ is the angle between the functions g and ψ in $L^2(D)$. Hence, (57) or (58) are also sufficient conditions of local optimality. In particular, (58) will be used in the algorithm described below.

4.2. The algorithm

The algorithm itself aims to generate a sequence $\{\psi_i\}$ of level-set functions (a sequence of structural domains $\{\Omega_i\}$) that will produce for some iteration

n a domain Ω_n such that (58) is satisfied to within a given small numerical tolerance $\epsilon_\theta > 0$:

$$\theta_n := \arccos\left[\frac{\langle g_n, \psi_n\rangle}{\|g_n\|_{L^2(D)}\,\|\psi_n\|_{L^2(D)}}\right] \leq \epsilon_\theta. \tag{59}$$

The iterative procedure starts with the choice of an initial guess for the optimal structure domain, i.e. with the choice of a starting level-set function $\psi_0 \in L^2(D)$. For simplicity, the function ψ_0 is chosen as a unit vector of $L^2(D)$. With $\mathcal{S}$ denoting the set of unit vectors of $L^2(D)$, the algorithm is explicitly given by

$$\begin{aligned} &\psi_0 \in \mathcal{S}, \\ &\psi_i = \frac{1}{\sin\theta_{i-1}}\left[\sin((1-\kappa_i)\theta_{i-1})\psi_{i-1} + \sin(\kappa_i\theta_{i-1})\frac{g_{i-1}}{\|g_{i-1}\|_{L^2(D)}}\right], \end{aligned} \tag{60}$$

where i denotes a generic iteration number and $\kappa_i \in [0,1]$ is a step size determined by a line-search performed at each iteration in order to decrease the value of the objective functional $I^\alpha_{\Omega_i}$. Note that the right hand side of $(60)_2$ is a convex combination between ψ_{i-1} and g_{i-1} up to a positive multiplicative constant and that, by construction of the iteration formula, we have

$$\psi_i \in \mathcal{S}. \tag{61}$$

The iterative process is stopped when for some iteration i the optimality condition (59) is satisfied to the desired degree of accuracy, i.e. if

$$\theta_i \leq \epsilon_\theta. \tag{62}$$

If at some iteration i, the line-search step size κ_i is found to be smaller than a given numerical tolerance $\epsilon_\kappa > 0$:

$$\kappa_i < \epsilon_\kappa, \tag{63}$$

i.e. if the topology is effectively no longer changing, and at the same time the optimality condition (62) is not met, then a uniform mesh refinement of the hold-all domain D is carried out and the iterative procedure is continued. The purpose of this coarse-to-fine procedure is twofold: on one hand it reduces the computer cost and, on the other hand, it makes the algorithm less prone to fall into (undesirable) local minima of high cost functional values. Of course,

as the continuum topology optimization problem has no global minimum in general, the mesh-dependency of the obtained optimized domain cannot be completely avoided. Note that a uniform mesh refinement will enrich the discretized space of level-set functions and will in general improve the accuracy of the elastic solutions. At this point we should add that more sophisticated approaches could be adopted, for example, by generating at each iteration a finite element mesh having element edges matching exactly the phase interface defined by the corresponding level-set function. Also, mesh density could be defined according to a suitable error estimator, leading to potential savings in computing time and ensuring the error is bounded to a desired level in the attained optimal structure domain. We emphasize, however, that our main purpose here is to demonstrate the robustness of the topological derivative-based iteration (60). Hence, we choose to rely on a simpler approach to avoid any potential lack of robustness being masked by procedures of a more peripheral nature.

In the computation of $D_T I_\Omega^\alpha$ according to expression (36) the stresses and the topological derivatives are first computed within the finite elements (at Gauss points) and then extrapolated to nodes. The final discretized version of the field $D_T I_\Omega^\alpha$ used in the iterations is generated by the finite element shape functions with smoothed nodal values obtained in a standard fashion. The level-set functions ψ and the discretized field $D_T I_\Omega^\alpha$ are generated by the same shape functions used in the finite element approximation of the direct and adjoint boundary value problems (3) and (51). The material properties E_{hard} or E_{soft} are assigned to nodes of the mesh depending on whether they are at points with $\psi < 0$ (hard phase) or $\psi > 0$ (soft phase). In this way, elements crossed by the hard-soft phase interface (defined by $\psi = 0$) will have Young's moduli between the values E_{hard} and E_{soft}, obtained by a standard interpolation of the nodal Young's moduli using the element shape functions. Obviously, according to the above procedure, the resolution of the optimal structure domain depends directly on the fineness of the adopted mesh. The overall optimization algorithm is conveniently summarized in Box 1 in pseudo-code format.

Remark 2. *The present procedure is* not *a member of the family usually referred to as* level-set methods *used, for instance, in [3]. The evolution of the level-set function in the so-called level-set method is governed by a Hamilton-Jacobi equation. Here the updated level-set function ψ_i at iteration i is obtained according to (60) and depends solely on the known level-set ψ_{i-1},*

the value κ_i, that produces a decrease in the value of the objective functional $I^{\alpha}_{\Omega_i}$, and the corresponding function g_{i-1}, which is constructed from the topological derivative field $D_T I^{\alpha}_{\Omega_{i-1}}$ for the known topology of iteration $i-1$. The computation of these quantities is straightforward and their computational implementation is simple.

Remark 3. *The only algorithmic parameters in addition to the tolerances ϵ_θ and ϵ_κ required by the present optimization algorithm are the penalty coefficient α, the penalty function parameter p and the compliance functional weighting factor β. The parameters α and p are chosen as large as possible and this choice is limited solely by numerical instabilities that result from excessively large values. Note, in particular, that* no artificial parameters or post-processing strategies *are required throughout the iterations. This is in contrast with existing SIMP-based structural optimization strategies and follows as a natural consequence of the use of the concept of topological derivative.*

Remark 4. *The solution of the adjoint equation* (51) *within the algorithm requires very little computational effort. Once the finite element solution for the elastic equilibrium problem* (3) *has been computed, the solution of* (51) *is obtained by only re-executing the back-substitution phase of the finite element procedure with the forcing term associated with the adjoint equation. All other calculations needed in the computation of the topological derivative, including the evaluation of* (49) *by means of a Gaussian quadrature, comprise only straightforward function evaluations. In practice, to avoid the repetitive calculation of Ψ_ρ according to* (49) *throughout the iterations, the function $\Psi_\rho(\boldsymbol{\sigma})$ is tabulated once and for all for a wide range of $\boldsymbol{\sigma}$ (range of principal values σ_I, σ_{II}) covering the normalized stress states usually encountered in the solution of the present class of problems. Throughout the optimization iterations, the required values of $\Psi_\rho(\boldsymbol{\sigma})$ are retrieved by interpolation of the tabulated values. The dominant computational cost at each iteration $(60)_2$ of the optimization algorithm is the solution of the elastic finite element equilibrium equations as many times as line-search iterations required to find the appropriate step size κ_i. Only a very small number of line-search iterations is commonly required.*

Box 1: Topological derivative-based algorithm for structural optimization with stress constraints.

(i) Initialize mesh counter, $j \leftarrow 1$; Generate a mesh of a chosen characteristic element size h_j for the hold-all domain D.

(ii) Initialize iteration counter, $i \leftarrow 0$; Choose an initial level-set function $\psi_0 \in \mathcal{S}$ defining the initial guess $\Omega_0 \subset D$ for the optimal structure domain.

(iii) Obtain the discretized fields $\boldsymbol{u}_{\Omega_i}$ and $\boldsymbol{v}_{\Omega_i}$ by solving, respectively, the elastic equilibrium problem (3) and the adjoint equation (51) for the current Ω_i with the current mesh h_j. Compute the corresponding value of $I^{\alpha}_{\Omega_i}$ according to (2).

(iv) Compute the topological derivative field $D_T I^{\alpha}_{\Omega_i}$ using expressions (36–50) and performing a standard nodal averaging procedure.

(v) Obtain the function g_i according to (55) using the nodal values of $D_T I^{\alpha}_{\Omega_i}$ and compute

$$\theta_i = \arccos\left[\frac{\langle g_n, \psi_n\rangle}{\|g_n\|_{L^2(D)}\,\|\psi_n\|_{L^2(D)}}\right]$$

(vi) IF $\theta_i \leq \epsilon_\theta$ THEN

EXIT (local optimum found!)

ELSE IF $(i > 0$ AND $\kappa_i < \epsilon_\kappa$ AND $\theta_i > \epsilon_\theta)$ THEN

Increment mesh counter, $j \leftarrow j + 1$;
Generate a new (finer) mesh for D with element size $h_j < h_{j-1}$;
GOTO (iii)

(vii) Increment iteration counter, $i \leftarrow i + 1$; Update level-set function:

$$\psi_i = \frac{1}{\sin\theta_{i-1}}\left[\sin((1-\kappa_i)\theta_{i-1})\psi_{i-1} + \sin(\kappa_i\theta_{i-1})\frac{g_{i-1}}{\|g_{i-1}\|_{L^2(D)}}\right]$$

(vii.a) In the above, perform a line-search to find κ_i such that

$$I^{\alpha}_{\Omega_i} < I^{\alpha}_{\Omega_{i-1}}$$

At each line-search iteration, compute the corresponding $\boldsymbol{u}_{\Omega_i}$ and $\boldsymbol{v}_{\Omega_i}$ by solving, respectively, the elastic problem (3) and the adjoint equation (51) for the associated Ω_i with the mesh h_j. Compute the corresponding value of $I^{\alpha}_{\Omega_i}$ according to (2).

(viii) GOTO (iv)

5. Numerical Examples

The effectiveness of the algorithm described above is demonstrated in this section by means of numerical examples. In order to avoid numerical ill-conditioning of the optimization problem we use in all examples, without loss of generality, a normalized version of the objective functional of (27) defined as

$$I_\Omega^\alpha(\boldsymbol{u}_\Omega) = \frac{|\Omega|}{V_0} + \frac{\beta}{K_0}\int_{\Gamma_N} \boldsymbol{g}\cdot\boldsymbol{u}_\Omega\, ds + \alpha\int_{\widetilde{D}} E_\Omega \Phi_p(\Upsilon(\boldsymbol{\sigma}(\boldsymbol{u}_\Omega)))\, d\boldsymbol{x}, \tag{64}$$

with the normalizing factors V_0 and K_0 being respectively the area and the compliance functional of the initial guess Ω_0 for the optimum structure domain, here taken as $\Omega_0 = D$. In all the examples, we adopt the Young's modulus contrast $E_{\text{soft}}/E_{\text{hard}} = 10^{-3}$.

5.1. Wall under shear load

The first example consists of wall under shear load (see Fig. 4).

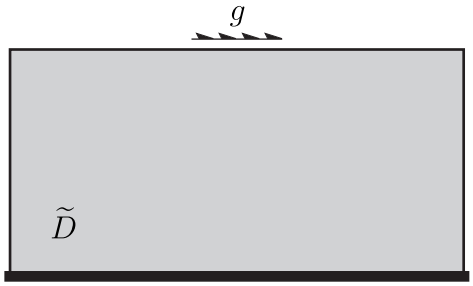

Figure 4: Wall under shear load. Initial guess and boundary conditions.

The hold-all domain is a rectangle of size 2×1 clamped at its bottom edge. The loading consists of a unit uniformly distributed horizontal force $\boldsymbol{g} = (1, 0)$ applied along a central portion of length 0.2 of the top edge of the hold-all domain. The material parameters $E_{\text{hard}} = 1.0$, $\nu = 0.3$ and $\overline{\sigma} = 1$ are used. For the penalty coefficient and compliance weighting factor we choose $\alpha = 25$ with $p = 32$ and $\beta = 1/4$. The optimization procedure is carried out for three different values of η. Firstly we use $\eta = 0$, corresponding to a von Mises stress constraint and then adopt $\eta = 0.4$ and $\eta = -0.4$. The positive η corresponds to a standard Drucker-Prager material with yield strength greater in compression than in tension. The negative value $\eta = -0.4$ models a

material with yield strength greater in tension than in compression. An initial uniform mesh containing 6400 linear triangles and 3321 nodes was adopted to discretize the hold-all domain. During the optimization procedure, one step of uniform mesh refinement of the hold-all domain (refer to item (vi) of Box 1) was required in all cases to achieve convergence with a tolerance $\epsilon_\theta = 1^\circ$. Convergence was attained in 26 iterations for the von Mises constraint case ($\eta = 0$) and 39 iterations in the other two cases ($\eta = 0.4$ and $\eta = -0.4$). The final mesh contains contains 25600 elements and 13041 nodes. The optimal topologies obtained are shown in Fig. 5.

(a) $\eta = 0.0$, volume fraction 40.34%

(b) $\eta = 0.4$, volume fraction 41.60%

(c) $\eta = -0.4$, volume fraction 41.60%

Figure 5: Wall under shear load. Obtained design for different values of η.

As one would expect, a symmetric structure is obtained under the von Mises constraint. The optimal domains for the other two cases are flipped

images of each other and, as expected, under the conventional Drucker-Prager constraint ($\eta = 0.4$) the member under compression (on the right) is bulkier than the member under tensile stresses (on the left).

5.2. L-bracket

Now we turn our attention to a classical structural optimization problem containing a geometrical singularity – the L-bracket problem subject to stress constraints. The hold-all domain and loading are illustrated in Fig. 6.

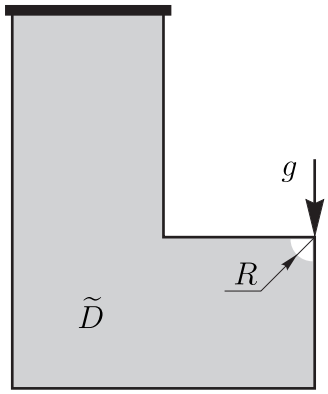

Figure 6: L-bracket. Initial guess and boundary condition.

This problem has been studied by a number of authors and various strategies have been proposed for the treatment of the von Mises stress constraint, exclusively in the context of SIMP-based methods of structural optimization (refer to [22] and references therein). The solution of this optimization problem (with a slightly different loading condition to that of Fig. 6) under a von Mises constraint by a topological derivative-based approach has been recently proposed in [8]. Here we show the application of the topological-derivative approach to the case of Drucker-Prager-type constraints. The lengths of the horizontal and vertical branches of the L-bracket are respectively 2 m and 2.5 m measured along their centre lines. Both have identical width of 1 m. The structure is clamped at the top edge and a point load $\boldsymbol{g} = -(0, 40)$ KN/m is applied to the corner of the right tip. The elastic properties of the structure material are $E_{\text{hard}} = 12500$ MPa and $\nu = 0.2$. The Drucker-Prager yield criterion parameters are set as $\eta = -0.3703$ and $\overline{\sigma}^{\star} = 63.85$ MPa. These are chosen so that the Drucker-Prager yield surface matches the compressive and tensile uniaxial yield strengths [13] of a natural wood, given respectively by

$f_c = 46.6\,\text{MPa}$ and $f_t = 101.4\,\text{MPa}$. The stress constraint is not enforced in the white region of radius $R = 0.15\,\text{m}$ directly under the point of load application (shown in Fig. 6). The initial (non-uniform) mesh discretizing the hold-all domain has 14236 three-noded triangular elements and 7323 nodes with a higher density of elements around the reentrant corner that gives rise to the stress singularity. Figure 7 shows the optimum structures obtained without and with the enforcement of the Drucker-Prager stress constraint.

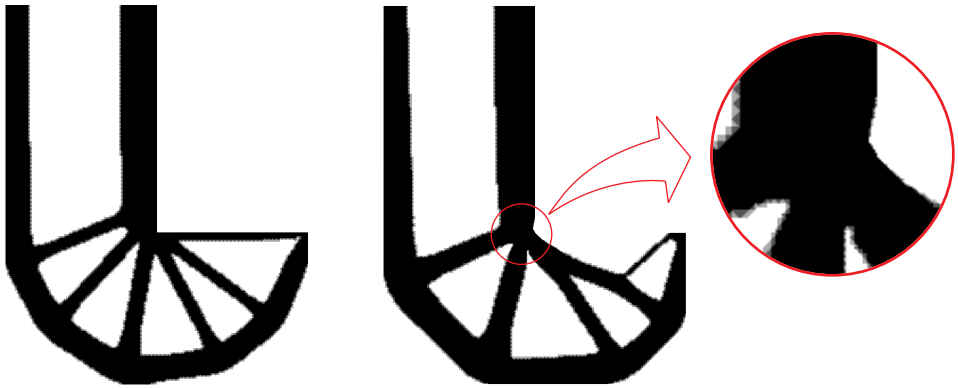

(a) unconstrained case (b) stress-constrained case

Figure 7: L-bracket. Obtained design for the unconstrained (volume fraction 42.96%) and constrained (volume fraction 46.76%) cases.

In the stress-constrained case, the penalty coefficient adopted in the penalized objective functional was $\alpha = 10^4$ with $p = 32$. In both cases we set $\beta = 1/3$. As in the previous example, one step of uniform mesh refinement (see item (vi) of Box 1) is performed in both cases to achieve convergence. The final mesh here has a total of 58240 elements and 29532 nodes. The convergence tolerance adopted for both unconstrained and stress-constrained problems is $\epsilon_\theta = 1^\circ$ with a total number of iterations required for convergence being 39 and 62, respectively. The evolution of the objective functional, volume fraction and angle θ throughout the iterations of the optimization algorithm is shown in Fig. 8(a–c).

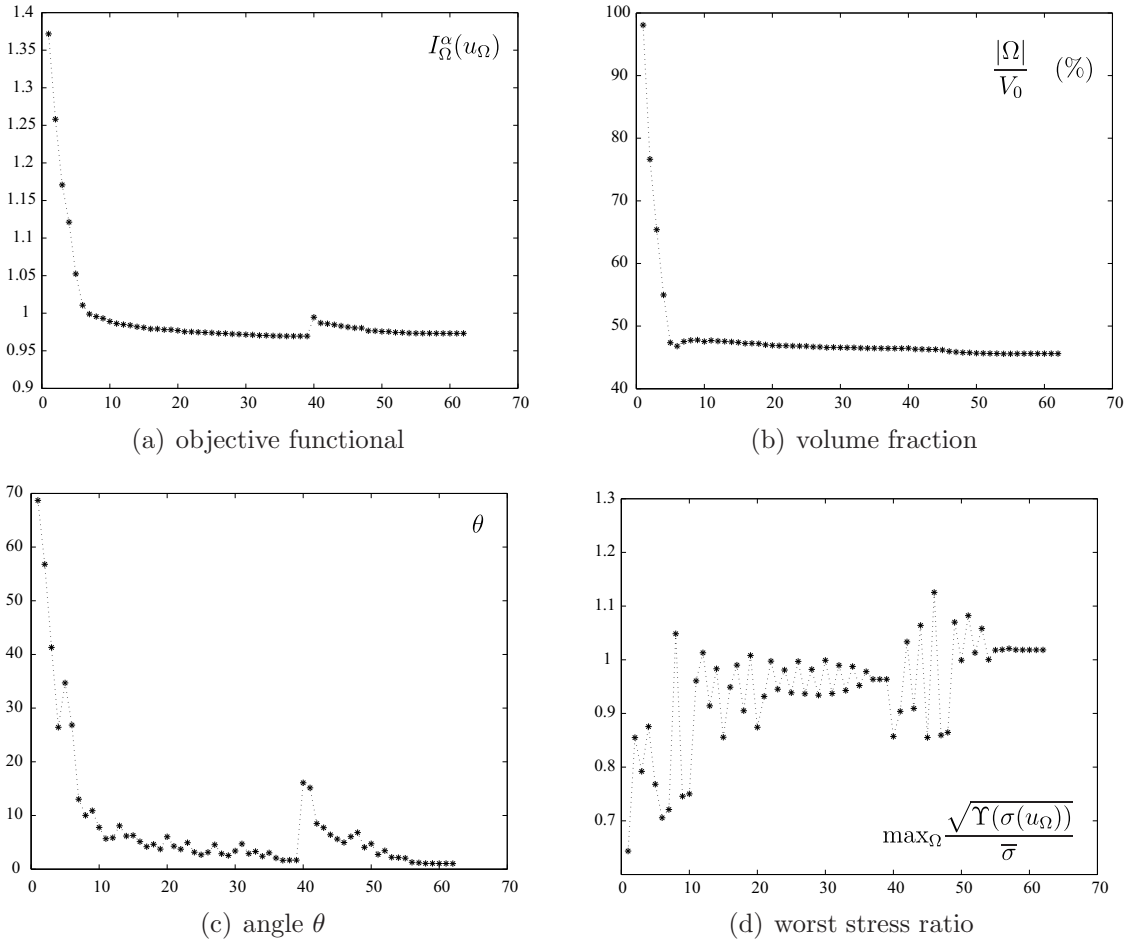

(a) objective functional (b) volume fraction

(c) angle θ (d) worst stress ratio

Figure 8: L-bracket. Convergence history.

We remark here that the adopted tolerances are quite stringent and a converged design for practical purposes is in fact obtained for the constrained case with the (quite satisfactory) initial mesh at iteration 39. This is where a sharp variation in θ and I^{α}_{Ω} is depicted in Figs. 8(a) and 8(c), corresponding to the mesh refinement step. Figure 8(d) shows the history of the worst stress ratio in the structure:

$$\max_\Omega \frac{\sqrt{\Upsilon(\sigma(u_\Omega))}}{\overline{\sigma}},$$

whose maximum admissible value is 1. It should be observed that in the stress constrained case shown in Fig. 7(b) the reentrant corner has been

rounded by the algorithm. The corresponding worst stress ratio in this case (shown in Fig. 8(d)) is 1.0184 for the converged structural domain – very close to its saturation value of 1. In the unconstrained case, on the other hand, the worst stress ratio blows up when minimizing the compliance due to the geometrical singularity of the reentrant corner.

It is worth noting here that the rounding off of the reentrant corner in the stress-constrained problem has been achieved by the present algorithm in a most natural manner *without any added post-processing techniques*. This is a mere consequence of the use of the exact formula (36) for the topological derivative of the objective functional. This formula gives the exact sensitivity of the penalized objective functional with respect to the considered black-and-white-type topological changes. The only approximation here is the use of a penalty term to enforce the required stress constraint. In SIMP-based methodologies on the other hand, some of the exact information on the sensitivity to black-and-white-type topological changes (i.e. first order terms of the topological asymptotic expansion of the objective functional) is inevitably lost with the introduction of the regularized density field that approximates the sharp black-white transition. The enforcement of stress constraints with such methods poses a more significant challenge and requires, for instance, the use of post-processing techniques to retrieve stresses. In this context, many such procedures have been proposed and used with success in a number of stress-constrained problems (a recent overview is provided in [22]).

5.3. Bridge design

This last example considers the design of a bridge. The hold-all domain is a rectangle 180 m long and 60 m high illustrated in Fig. 9.

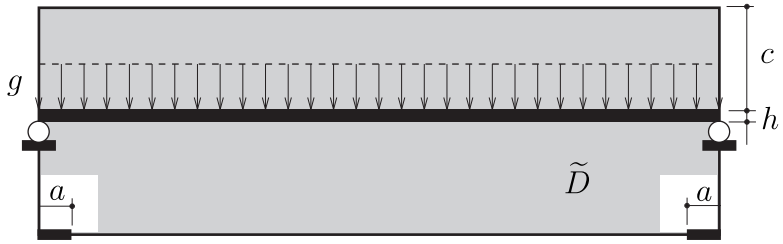

Figure 9: Bridge design. Initial guess and boundary conditions.

The bridge is assumed clamped at the two bottom supports of equal length $a = 9\,\mathrm{m}$. A uniformly distributed traffic load $\boldsymbol{g} = -(0, 400)\,\mathrm{KN/m^2}$ is

applied to the edge of the dark strip of height $h = 3\,\mathrm{m}$ indicated in Fig. 9 that represents the road and will remain unchanged throughout the optimization process. The strip is positioned at a distance $c = 27\,\mathrm{m}$ from the top of the hold-all domain. The material properties are $E_{\mathrm{hard}} = 27500\,\mathrm{MPa}$ and $\nu = 0.2$. For the purpose of comparison, the optimization procedure is carried for two cases: (a) No stress constraints ($\alpha = 0$), and (b) The Drucker-Prager stress constraint with yield strength parameters $\eta = 0.417$ and $\overline{\sigma}^{\star} = 5.05\,\mathrm{MPa}$. These parameters are obtained from the Drucker-Prager biaxial fit model [13] to match a tensile and compressive yield strength of $f_c = 30.5\,\mathrm{MPa}$ and $f_t = 2.75\,\mathrm{MPa}$ respectively. For the stress-constrained case we adopt the penalty coefficient $\alpha = 10^3$ and in both cases we choose $\beta = 1/10$ and the convergence tolerance $\epsilon_\theta = 1^\circ$. The stress constraint is not enforced within the white region of size $15 \times 15\mathrm{m}$ adjacent to the bottom supports. Due to symmetry, only half of the hold-all domain is discretized. The initial (uniform) mesh has 4800 elements and 2501 nodes. In both cases, two steps of uniform mesh refinement are performed leading to a final mesh of 76800 and 38801 nodes. Figure 10 shows the optimized topologies obtained for the two cases.

(a) Unconstrained case

(b) Stress-constrained case

Figure 10: Bridge design. Obtained design for the unconstrained and constrained cases.

The total number of iteration required for convergence was 16 and 13, respectively, for the unconstrained and constrained cases. Note that the unconstrained optimization results in the well-known tie-arch bridge design.

In this design some structural members are under tensile and others under compressive dominant stresses. The stress-constrained optimization with the Drucker-Prager criterion, on the other hand, results in a radically different design where all members are subject to compressive dominant stresses. Such designs are typical in practice for materials whose compressive strength is much higher than their tensile strength (such as concrete). Its automatic generation here clearly demonstrates the success of the proposed topology optimization procedure.

6. Conclusion

This paper has extended the result derived in [8] to incorporate the Drucker-Prager stress constraint within a topological derivative-based algorithm for topology optimization of elastic structures. In this context a penalty functional has been proposed to enforce the point-wise Drucker-Prager constraint and a closed formula for its topological derivative has been presented. The overall algorithm, which uses the topological derivative to indicate the descent direction in conjunction with a level-set representation of the structure domain, is of remarkably simple computational implementation. In particular, it does not feature post-processing procedures (such as filtering or relaxation) of any kind and only a minimal number of user-defined algorithmic parameters are needed. This is in sharp contrast with current methodologies of topological structural optimization with local stress constraints. Numerical examples have demonstrated the effectiveness and efficiency of the algorithm in the solution of topology optimization problems under the considered class of constraints. The algorithm was shown, for instance, to efficiently handle topology optimization with materials displaying strong asymmetry in their tensile and compressive uniaxial yield strengths. From a practical standpoint, we believe this fact to be particularly relevant in that it opens the possibility for the efficient automatic design/optimization of structures made of a much wider range of materials than that for which stress-constrained topology optimization has been mainly used so far. The extension of the present work to the three-dimensional case is currently under investigation.

Appendix A. Topological sensitivity analysis of the Drucker-Prager stress penalty functional

The topological derivative of the penalty functional J_Ω defined in (22) and taking part in the rightmost term of (36) is derived here in detail. Recall that the class of topological perturbations of Ω considered here consist of the introduction of a circular inclusion $B_\varepsilon(\widehat{\boldsymbol{x}})$ of radius ε and center at an arbitrary point $\widehat{\boldsymbol{x}} \in D \setminus \partial\Omega$, as defined in (35) (refer to Fig. A.11). Possibly shifting the origin of the coordinate system, we assume for simplicity and without loss of generality that $\widehat{\boldsymbol{x}} = 0$. For all $\varepsilon \geq 0$, the state equations can be rewritten as:

$$\left\{ \begin{array}{rcll} -\mathrm{div}\,(\gamma_\varepsilon \boldsymbol{\sigma}(\boldsymbol{u}_\varepsilon)) &=& 0 \quad \text{in} & D, \\ \boldsymbol{u}_\varepsilon &=& 0 \quad \text{on} & \Gamma_D, \\ \gamma_\varepsilon \boldsymbol{\sigma}(\boldsymbol{u}_\varepsilon)\,\boldsymbol{n} &=& \boldsymbol{g} \quad \text{on} & \Gamma_N, \\ \boldsymbol{\sigma}(\boldsymbol{u}_\varepsilon)\,\boldsymbol{n} &=& 0 \quad \text{on} & \Gamma_0, \end{array} \right. \tag{A.1}$$

where we have introduced the notations $\boldsymbol{u}_\varepsilon := \boldsymbol{u}_{\Omega_\varepsilon}$ and

$$\gamma_\varepsilon = \left\{ \begin{array}{ll} \gamma_0 \quad \text{in} & D \setminus \overline{B_\varepsilon}, \\ \gamma_1 \quad \text{in} & B_\varepsilon. \end{array} \right. \tag{A.2}$$

We assume that $\gamma_0 := E_\Omega$ and $\gamma_1 := \gamma E_\Omega$, with the contrast γ given by (42), are two positive functions defined in D and constant in a neighborhood of $\widehat{\boldsymbol{x}}$.

In order to derive a closed formula for the topological derivative $D_T J_\Omega$ we need to obtain a topological asymptotic expansion of the form

$$J_\varepsilon(\boldsymbol{u}_\varepsilon) - J_0(\boldsymbol{u}_0) = f(\varepsilon) D_T J_\Omega + o(f(\varepsilon)), \tag{A.3}$$

where the function f has already been identified in Sections 3.1 and 3.2 as $f(\varepsilon) = \varepsilon^2$ and, for simplicity in the derivation that follows, we adopt the notation $\boldsymbol{u}_0 := \boldsymbol{u}_\Omega$, $J_0 := J_\Omega$ and

$$J_\varepsilon(\boldsymbol{u}) := J_{\Omega_\varepsilon}(\boldsymbol{u}) = \int_{\widetilde{D}} \gamma_\varepsilon \Phi(\Upsilon(\boldsymbol{\sigma}(\boldsymbol{u}))) d\boldsymbol{x}. \tag{A.4}$$

In obtaining the above topological asymptotic expansion, we shall follow the approach described in [6] for the Laplace problem. Here, however, the calculations are more elaborate but the estimates of the remainders, i.e. the terms of higher order in $f(\varepsilon)$ gathered in the rightmost term of the right hand side of (A.3), are analogous to those of [6]. Hence in what follows we shall

skip the calculation of the estimates. The reader interested in the complete proofs may refer to [6]. We start by stating the following important result, whose proof can be found in [4]:

Proposition 5. *Let $\mathcal{V}$ be a linear space and $\varepsilon_0 > 0$. For all $\varepsilon \in [0, \varepsilon_0)$, consider a vector $\boldsymbol{u}_\varepsilon \in \mathcal{V}$ solution of a variational problem of the form*

$$a_\varepsilon(\boldsymbol{u}_\varepsilon, \boldsymbol{v}) = \ell_\varepsilon(\boldsymbol{v}) \quad \forall \boldsymbol{v} \in \mathcal{V}, \tag{A.5}$$

where a_ε and ℓ_ε are, respectively, a bilinear and a linear form on $\mathcal{V}$. Consider also, for all $\varepsilon \in [0, \varepsilon_0)$, a functional $J_\varepsilon : \mathcal{V} \to \Re$ and a linear form $L_\varepsilon(\boldsymbol{u}_0) \in \mathcal{V}'$. Assume that the following hypotheses hold:

1. *There exist two numbers δa and $\delta \ell$ and a function $\varepsilon \in \Re_+ \mapsto f(\varepsilon) \in \Re$ such that, when ε goes to zero,*

$$\begin{aligned} (a_\varepsilon - a_0)(\boldsymbol{u}_0, \boldsymbol{v}_\varepsilon) &= f(\varepsilon)\delta a + o(f(\varepsilon)), & \text{(A.6)} \\ (\ell_\varepsilon - \ell_0)(\boldsymbol{v}_\varepsilon) &= f(\varepsilon)\delta \ell + o(f(\varepsilon)), & \text{(A.7)} \\ \lim_{\varepsilon \to 0} f(\varepsilon) &= 0. & \text{(A.8)} \end{aligned}$$

   Following standard convention, $(a_\varepsilon - a_0)(\boldsymbol{u}_0, \boldsymbol{v}_\varepsilon) = a_\varepsilon(\boldsymbol{u}_0, \boldsymbol{v}_\varepsilon) - a_0(\boldsymbol{u}_0, \boldsymbol{v}_\varepsilon)$ and $(\ell_\varepsilon - \ell_0)(\boldsymbol{v}_\varepsilon) = \ell_\varepsilon(\boldsymbol{v}_\varepsilon) - \ell_0(\boldsymbol{v}_\varepsilon)$, where $\boldsymbol{v}_\varepsilon \in \mathcal{V}$ is solution to the following auxiliary problem (the standard adjoint state associated with (A.4) when $\varepsilon = 0$):

$$a_\varepsilon(\boldsymbol{\varphi}, \boldsymbol{v}_\varepsilon) = -\langle L_\varepsilon(\boldsymbol{u}_0), \boldsymbol{\varphi} \rangle \quad \forall \boldsymbol{\varphi} \in \mathcal{V}. \tag{A.9}$$

2. *There exist two numbers δJ_1 and δJ_2 such that*

$$\begin{aligned} J_\varepsilon(\boldsymbol{u}_\varepsilon) &= J_\varepsilon(\boldsymbol{u}_0) + \langle L_\varepsilon(\boldsymbol{u}_0), \boldsymbol{u}_\varepsilon - \boldsymbol{u}_0 \rangle + f(\varepsilon)\delta J_1 + o(f(\varepsilon)), & \text{(A.10)} \\ J_\varepsilon(\boldsymbol{u}_0) &= J_0(\boldsymbol{u}_0) + f(\varepsilon)\, \delta J_2 + o(f(\varepsilon)). & \text{(A.11)} \end{aligned}$$

Then we have

$$J_\varepsilon(\boldsymbol{u}_\varepsilon) - J_0(\boldsymbol{u}_0) = f(\varepsilon)(\delta a - \delta \ell + \delta J_1 + \delta J_2) + o(f(\varepsilon)). \tag{A.12}$$

The bilinear and linear forms associated with Problem (A.1) are classically defined in the space $\mathcal{V}$ given by (6) as follows:

$$\begin{aligned} a_\varepsilon(\boldsymbol{u}, \boldsymbol{v}) &= \int_D \gamma_\varepsilon \boldsymbol{\sigma}(\boldsymbol{u}) \cdot \boldsymbol{e}(\boldsymbol{v})\, d\boldsymbol{x} \qquad \forall \boldsymbol{u}, \boldsymbol{v} \in \mathcal{V}, & \text{(A.13)} \\ \ell_\varepsilon(\boldsymbol{v}) &= \int_{\Gamma_N} \boldsymbol{g} \cdot \boldsymbol{u}\, ds \qquad \forall \boldsymbol{u} \in \mathcal{V}. & \text{(A.14)} \end{aligned}$$

At the point $\boldsymbol{u}_0$ of $\mathcal{V}$ (solution of the state equations for the unperturbed domain), the penalty functional admits the tangent linear approximation $L_\varepsilon(\boldsymbol{u}_0)$ given by:

$$\langle L_\varepsilon(\boldsymbol{u}_0), \boldsymbol{\varphi}\rangle = \int_{\widetilde{D}} \gamma_\varepsilon k_1(\boldsymbol{u}_0)[\mathbb{B}\boldsymbol{\sigma}(\boldsymbol{u}_0)\cdot\boldsymbol{e}(\boldsymbol{\varphi}) + \xi\,\mathrm{tr}\boldsymbol{e}(\boldsymbol{\varphi})]d\boldsymbol{x} \qquad \forall \boldsymbol{\varphi}\in\mathcal{V}, \tag{A.15}$$

where k_1 is defined in (45). Then the adjoint state is a (weak) solution of the boundary value problem:

$$\left\{\begin{array}{rcll} -\mathrm{div}\,(\gamma_\varepsilon\boldsymbol{\sigma}(\boldsymbol{v}_\varepsilon)) &=& \mathrm{div}\,[\gamma_\varepsilon k_1(\boldsymbol{u}_0)(\mathbb{B}\boldsymbol{\sigma}(\boldsymbol{u}_0)+\xi\boldsymbol{I})] & \text{in } D,\\ \boldsymbol{v}_\varepsilon &=& 0 & \text{on } \Gamma_D,\\ \gamma_\varepsilon\boldsymbol{\sigma}(\boldsymbol{v}_\varepsilon)\,\boldsymbol{n} &=& -\gamma_\varepsilon k_1(\boldsymbol{u}_0)(\mathbb{B}\boldsymbol{\sigma}(\boldsymbol{u}_0)+\xi\boldsymbol{I})\boldsymbol{n} & \text{on } \Gamma_N\cup\Gamma_0,\\ [\![\gamma_\varepsilon\boldsymbol{\sigma}(\boldsymbol{v}_\varepsilon)]\!]\boldsymbol{n} &=& -[\![\gamma_\varepsilon k_1(\boldsymbol{u}_0)(\mathbb{B}\boldsymbol{\sigma}(\boldsymbol{u}_0)+\xi\boldsymbol{I})]\!]\boldsymbol{n} & \text{on } \partial B_\varepsilon, \end{array}\right. \tag{A.16}$$

where $[\![\gamma_\varepsilon\boldsymbol{\sigma}(\boldsymbol{v}_\varepsilon)]\!]\boldsymbol{n}$ denotes the jump of the normal stress across the interface ∂B_ε. Before proceeding, we make the following assumptions:

1. For any $r_1 > 0$ there exists $r_2 \in (0, r_1)$ such that every function $\boldsymbol{u} \in H^1(D \setminus \overline{B(\widehat{\boldsymbol{x}}, r_2)})^2$ satisfying

$$\left\{\begin{array}{rcll} -\mathrm{div}\,(\gamma_0\boldsymbol{\sigma}(\boldsymbol{u})) &=& 0 & \text{in } D\setminus\overline{B(\widehat{\boldsymbol{x}},r_2)},\\ \boldsymbol{u} &=& 0 & \text{on } \Gamma_D,\\ \gamma_0\boldsymbol{\sigma}(\boldsymbol{u})\,\boldsymbol{n} &=& 0 & \text{on } \Gamma_N\cup\Gamma_0 \end{array}\right. \tag{A.17}$$

   belongs to $W^{1,4}(\widetilde{D}\setminus\overline{B(\widehat{\boldsymbol{x}},r_1)})^2$.
2. The load $\boldsymbol{g}$ is such that $\boldsymbol{u}_0 \in W^{1,4}(\widetilde{D})^2$.

And we also note that, by elliptic regularity, $\boldsymbol{u}_0$ and $\boldsymbol{v}_0$ are automatically of class $\mathcal{C}^{1,\beta}$, $\beta > 0$, in the vicinity of $\widehat{\boldsymbol{x}}$ provided that $\widehat{\boldsymbol{x}} \in D \setminus \partial\Omega \setminus \partial\widetilde{D}$.

Remark 6. *The above assumption is satisfied in many situations, including non-smooth domains such as, for instance, in the following case:*

- *D is a Lipschitz polygon,*
- *$\Gamma_N \cap \partial\widetilde{D} = \emptyset$ and $\Gamma_D \cap \partial\widetilde{D} = \emptyset$,*
- *the interface $\partial\Omega \setminus \partial D$ is the disjoint union of smooth simple arcs,*

- *if a junction point between the interface and ∂D belongs to $\partial\widetilde{D}$, then the Young modulus distribution around this point is quasi-monotone (see the definition in [21]); in particular, if only one arc touches ∂D at this point, it is sufficient that the angle defined by these curves in $D \setminus \overline{\Omega}$ is less than π.*

We refer to [21] and the references therein for justifications and extensions.

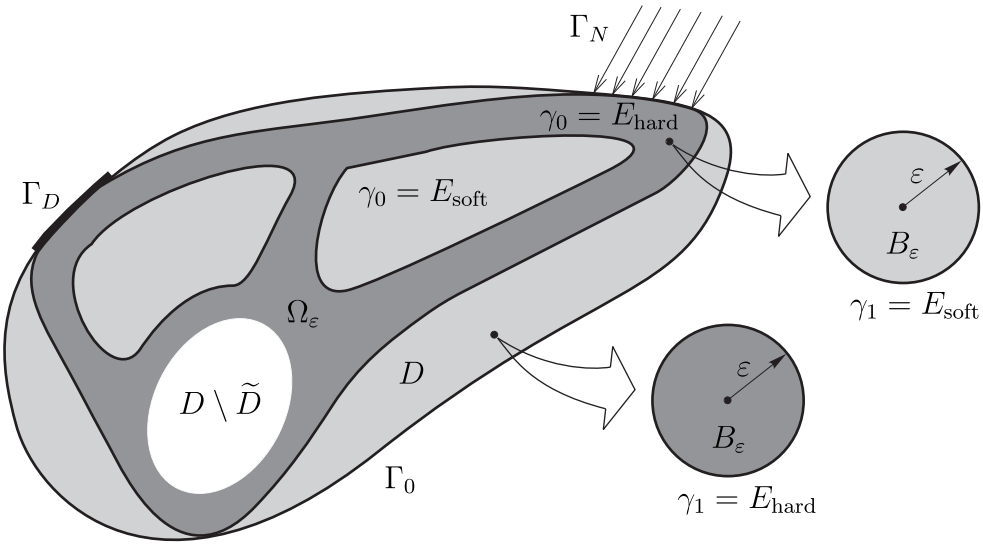

Figure A.11: Topologically perturbed domain.

Appendix A.1. Variation of the bilinear form

In order to make use of the result of Proposition 5, we need to obtain a closed formula for the leading term of the variation of the bilinear form

$$(a_\varepsilon - a_0)(\boldsymbol{u}_0, \boldsymbol{v}_\varepsilon) = \int_{B_\varepsilon} (\gamma_1 - \gamma_0)\boldsymbol{\sigma}(\boldsymbol{u}_0) \cdot \boldsymbol{e}(\boldsymbol{v}_\varepsilon) d\boldsymbol{x}. \tag{A.18}$$

In deriving the closed formula, we shall denote $\mathcal{E}_i(\varepsilon)$, $i = 1, 2, ...$, the remainders – terms of higher order in $f(\varepsilon)$:

$$\lim_{\varepsilon \to 0} \frac{\mathcal{E}_i(\varepsilon)}{f(\varepsilon)} = 0 \tag{A.19}$$

– identified in (A.18). By setting $\widetilde{\boldsymbol{v}}_\varepsilon := \boldsymbol{v}_\varepsilon - \boldsymbol{v}_0$, with $\boldsymbol{v}_0 := \boldsymbol{v}_\Omega$, and assuming that ε is sufficiently small so that γ_ε is constant in B_ε, we obtain:

$$(a_\varepsilon - a_0)(\boldsymbol{u}_0, \boldsymbol{v}_\varepsilon) = (\gamma_1 - \gamma_0)(\widehat{\boldsymbol{x}}) \left(\int_{B_\varepsilon} \boldsymbol{\sigma}(\boldsymbol{u}_0) \cdot \boldsymbol{e}(\boldsymbol{v}_0) d\boldsymbol{x} + \int_{B_\varepsilon} \boldsymbol{\sigma}(\boldsymbol{u}_0) \cdot \boldsymbol{e}(\widetilde{\boldsymbol{v}}_\varepsilon) d\boldsymbol{x} \right). \tag{A.20}$$

Since $\boldsymbol{u}_0$ and $\boldsymbol{v}_0$ are smooth in the vicinity of $\widehat{\boldsymbol{x}}$, we approximate $\sigma(\boldsymbol{u}_0)$ and $\boldsymbol{e}(\boldsymbol{v}_0)$ in the first integral by their values at the point $\widehat{\boldsymbol{x}}$, and write:

$$(a_\varepsilon - a_0)(\boldsymbol{u}_0, \boldsymbol{v}_\varepsilon) = (\gamma_1 - \gamma_0)(\widehat{\boldsymbol{x}}) \left(\pi \varepsilon^2 \boldsymbol{\sigma}(\boldsymbol{u}_0)(\widehat{\boldsymbol{x}}) \cdot \boldsymbol{e}(\boldsymbol{v}_0)(\widehat{\boldsymbol{x}}) + \int_{B_\varepsilon} \boldsymbol{\sigma}(\boldsymbol{u}_0) \cdot \boldsymbol{e}(\widetilde{\boldsymbol{v}}_\varepsilon) d\boldsymbol{x} + \mathcal{E}_1(\varepsilon) \right). \tag{A.21}$$

As $\boldsymbol{v}_\varepsilon$ is solution of the adjoint equation (A.16), the function $\widetilde{\boldsymbol{v}}_\varepsilon$ solves

$$\left\{ \begin{array}{rcll} -\mathrm{div}(\gamma_\varepsilon \boldsymbol{\sigma}(\widetilde{\boldsymbol{v}}_\varepsilon)) & = & 0 & \text{in} \quad B_\varepsilon \cup (D \setminus \overline{B_\varepsilon}), \\ [\![\gamma_\varepsilon \boldsymbol{\sigma}(\widetilde{\boldsymbol{v}}_\varepsilon)\, \boldsymbol{n}]\!] & = & -(\gamma_1 - \gamma_0) \left[k_1(\boldsymbol{u}_0)(\mathbb{B}\boldsymbol{\sigma}(\boldsymbol{u}_0) + \xi \boldsymbol{I}) + \boldsymbol{\sigma}(\boldsymbol{v}_0) \right] \boldsymbol{n} & \text{on} \quad \partial B_\varepsilon, \\ \widetilde{\boldsymbol{v}}_\varepsilon & = & 0 & \text{on} \quad \Gamma_D, \\ \boldsymbol{\sigma}(\widetilde{\boldsymbol{v}}_\varepsilon)\, \boldsymbol{n} & = & 0 & \text{on} \quad \Gamma_N \cup \Gamma_0. \end{array} \right. \tag{A.22}$$

We recall that, as before, the boundary value problem (A.22) is to be understood in the weak sense for $\widetilde{\boldsymbol{v}}_\varepsilon \in H^1(D)^2$. We set $\boldsymbol{S} := \boldsymbol{S}_1 + \boldsymbol{S}_2$, with

$$\boldsymbol{S}_1 := k_1(\boldsymbol{u}_0)(\widehat{\boldsymbol{x}})(\mathbb{B}\boldsymbol{\sigma}(\boldsymbol{u}_0)(\widehat{\boldsymbol{x}}) + \xi \boldsymbol{I}) \qquad \text{and} \qquad \boldsymbol{S}_2 := \boldsymbol{\sigma}(\boldsymbol{v}_0)(\widehat{\boldsymbol{x}}). \tag{A.23}$$

We approximate $\boldsymbol{\sigma}(\widetilde{\boldsymbol{v}}_\varepsilon)$ by $\boldsymbol{\sigma}(\boldsymbol{h}_\varepsilon^S)$ – solution of the following auxiliary problem:

$$\left\{ \begin{array}{rcll} -\mathrm{div}(\boldsymbol{\sigma}(\boldsymbol{h}_\varepsilon^S)) & = & 0 & \text{in} \quad B_\varepsilon \cup (\Re^2 \setminus \overline{B_\varepsilon}), \\ [\![\gamma_\varepsilon \boldsymbol{\sigma}(\boldsymbol{h}_\varepsilon^S)]\!]\, \boldsymbol{n} & = & -(\gamma_1 - \gamma_0)\, (\widehat{\boldsymbol{x}})\, \boldsymbol{S}\boldsymbol{n} & \text{on} \quad \partial B_\varepsilon, \\ \boldsymbol{\sigma}(\boldsymbol{h}_\varepsilon^S) & \to & 0 & \text{at} \quad \infty, \end{array} \right. \tag{A.24}$$

In the present case of a circular inclusion, the tensor field $\boldsymbol{\sigma}(\boldsymbol{h}_\varepsilon^S)$ that solves the exterior problem (A.24) has the following classical expression [23] in a polar coordinate system (r, θ):

- for $r \geq \varepsilon$

$$\begin{aligned}
\sigma_r(r,\theta) &= -(\alpha_1+\alpha_2)\frac{1-\gamma}{1+a\gamma}\frac{\varepsilon^2}{r^2} \\
&- \frac{1-\gamma}{1+b\gamma}\left(4\frac{\varepsilon^2}{r^2}-3\frac{\varepsilon^4}{r^4}\right)(\beta_1\cos 2\theta+\beta_2\cos 2(\theta+\phi)), \quad \text{(A.25)} \\
\sigma_\theta(r,\theta) &= (\alpha_1+\alpha_2)\frac{1-\gamma}{1+a\gamma}\frac{\varepsilon^2}{r^2} \\
&- 3\frac{1-\gamma}{1+b\gamma}\frac{\varepsilon^4}{r^4}(\beta_1\cos 2\theta+\beta_2\cos 2(\theta+\phi)), \quad \text{(A.26)} \\
\sigma_{r\theta}(r,\theta) &= -\frac{1-\gamma}{1+b\gamma}\left(2\frac{\varepsilon^2}{r^2}-3\frac{\varepsilon^4}{r^4}\right)(\beta_1\sin 2\theta+\beta_2\sin 2(\theta+\phi)), \quad \text{(A.27)}
\end{aligned}$$

- for $0 < r < \varepsilon$

$$\begin{aligned}
\sigma_r(r,\theta) &= (\alpha_1+\alpha_2)\,a\frac{1-\gamma}{1+a\gamma} \\
&+ b\frac{1-\gamma}{1+b\gamma}(\beta_1\cos 2\theta+\beta_2\cos 2(\theta+\phi)), \quad \text{(A.28)} \\
\sigma_\theta(r,\theta) &= (\alpha_1+\alpha_2)\,a\frac{1-\gamma}{1+a\gamma} \\
&- b\frac{1-\gamma}{1+b\gamma}(\beta_1\cos 2\theta+\beta_2\cos 2(\theta+\phi)), \quad \text{(A.29)} \\
\sigma_{r\theta}(r,\theta) &= -b\frac{1-\gamma}{1+b\gamma}(\beta_1\sin 2\theta+\beta_2\sin 2(\theta+\phi)), \quad \text{(A.30)}
\end{aligned}$$

Some terms in the above formulas require explanation. The parameter ϕ denotes the angle between the eigenvectors of the tensors $\boldsymbol{S}_1$ and $\boldsymbol{S}_2$,

$$\alpha_i = \frac{1}{2}(s_I^i + s_{II}^i) \quad \text{and} \quad \beta_i = \frac{1}{2}(s_I^i - s_{II}^i), \quad i = 1,2, \tag{A.31}$$

where s_I^i and s_{II}^i are the eigenvalues of the tensors $\boldsymbol{S}_i$ for $i = 1, 2$. In addition, the constants a and b are given by (43) and γ is the contrast, defined in (42), evaluated at $\widehat{\boldsymbol{x}}$.

From the above, we obtain successively:

$$\int_{B_\varepsilon} \boldsymbol{\sigma}(\boldsymbol{u}_0)\cdot\boldsymbol{e}(\widetilde{\boldsymbol{v}}_\varepsilon)d\boldsymbol{x} = \int_{B_\varepsilon} \boldsymbol{\sigma}(\widetilde{\boldsymbol{v}}_\varepsilon)\cdot\boldsymbol{e}(\boldsymbol{u}_0)d\boldsymbol{x} = \int_{B_\varepsilon} \boldsymbol{\sigma}(\boldsymbol{h}_\varepsilon^S)\cdot\boldsymbol{e}(\boldsymbol{u}_0)d\boldsymbol{x} + \mathcal{E}_2(\varepsilon). \tag{A.32}$$

Then, by approximating $\boldsymbol{e}(\boldsymbol{u}_0)$ in B_ε by its value at $\widehat{\boldsymbol{x}}$ and calculating the resulting integral with the help of the expressions (A.28)-(A.30), we get

$$\begin{aligned}\int_{B_\varepsilon} \boldsymbol{\sigma}(\boldsymbol{u}_0)\cdot\boldsymbol{e}(\widetilde{\boldsymbol{v}}_\varepsilon)d\boldsymbol{x} &= \int_{B_\varepsilon} \boldsymbol{\sigma}(h_\varepsilon^S)\cdot\boldsymbol{e}(\boldsymbol{u}_0)(\widehat{\boldsymbol{x}})d\boldsymbol{x} + \mathcal{E}_2(\varepsilon)+\mathcal{E}_3(\varepsilon)\\ &= -\pi\varepsilon^2\rho\,[k_1(\boldsymbol{u}_0)\mathbb{T}(\mathbb{B}\boldsymbol{\sigma}(\boldsymbol{u}_0)+\xi\boldsymbol{I})\cdot\boldsymbol{e}(\boldsymbol{u}_0)\\ &\quad + \mathbb{T}\boldsymbol{\sigma}(\boldsymbol{u}_0)\cdot\boldsymbol{e}(\boldsymbol{v}_0)]\,(\widehat{\boldsymbol{x}}) + \mathcal{E}_2(\varepsilon)+\mathcal{E}_3(\varepsilon),\end{aligned} \tag{A.33}$$

with ρ and $\mathbb{T}$ given by (40) and (41), respectively.

Finally, the variation of the bilinear form can be written as:

$$\begin{aligned}(a_\varepsilon - a_0)(\boldsymbol{u}_0,\boldsymbol{v}_\varepsilon) = -\pi\varepsilon^2(\gamma_1-\gamma_0)(\widehat{\boldsymbol{x}})\rho\Big(k_1(\boldsymbol{u}_0)b(\mathbb{B}\boldsymbol{\sigma}(\boldsymbol{u}_0)+\xi\boldsymbol{I})\cdot\boldsymbol{e}(\boldsymbol{u}_0)+\\ k_1(\boldsymbol{u}_0)\frac{a-b}{2(1+\gamma a)}\mathrm{tr}[\mathbb{B}\boldsymbol{\sigma}(\boldsymbol{u}_0)+\xi\boldsymbol{I}]\,\mathrm{tr}\boldsymbol{e}(\boldsymbol{u}_0)-\\ \frac{b+1}{\gamma-1}\boldsymbol{\sigma}(\boldsymbol{u}_0)\cdot\boldsymbol{e}(\boldsymbol{v}_0)+\frac{a-b}{2(1+\gamma a)}\mathrm{tr}\boldsymbol{\sigma}(\boldsymbol{u}_0)\,\mathrm{tr}\boldsymbol{e}(\boldsymbol{v}_0)\Big)(\widehat{\boldsymbol{x}})+(\gamma_1-\gamma_0)(\widehat{\boldsymbol{x}})\sum_{i=1}^{3}\mathcal{E}_i(\varepsilon).\end{aligned} \tag{A.34}$$

Appendix A.2. Variation of the linear form

Since here ℓ_ε is independent of ε, it follows trivially that

$$(\ell_\varepsilon - \ell_0)(\boldsymbol{v}_\varepsilon) = 0. \tag{A.35}$$

Appendix A.3. Partial variation of the penalty functional with respect to the state

We now focus on the variation:

$$V_{J1}(\varepsilon) = J_\varepsilon(\boldsymbol{u}_\varepsilon) - J_\varepsilon(\boldsymbol{u}_0) - \langle L_\varepsilon(\boldsymbol{u}_0), \boldsymbol{u}_\varepsilon - \boldsymbol{u}_0\rangle, \tag{A.36}$$

which in view of the definition of J_ε and L_ε reads

$$\begin{aligned}V_{J1}(\varepsilon) = \int_{\widetilde{D}} \gamma_\varepsilon\,[\Phi(\Upsilon(\boldsymbol{\sigma}(\boldsymbol{u}_\varepsilon))) - \Phi(\Upsilon(\boldsymbol{\sigma}(\boldsymbol{u}_0))) -\\ \Phi'(\Upsilon(\boldsymbol{\sigma}(\boldsymbol{u}_0)))(\mathbb{B}\boldsymbol{\sigma}(\boldsymbol{u}_0)\cdot\boldsymbol{e}(\boldsymbol{u}_\varepsilon-\boldsymbol{u}_0)+\xi\mathrm{tr}\boldsymbol{e}(\boldsymbol{u}_\varepsilon-\boldsymbol{u}_0))]\,d\boldsymbol{x}.\end{aligned} \tag{A.37}$$

By setting $\widetilde{\boldsymbol{u}}_\varepsilon = \boldsymbol{u}_\varepsilon - \boldsymbol{u}_0$, we can re-write:

$$V_{J1}(\varepsilon) = \int_{\widetilde{D}} \gamma_\varepsilon \Big[\Phi(\Upsilon(\boldsymbol{\sigma}(\boldsymbol{u}_0)) + \mathbb{B}\boldsymbol{\sigma}(\boldsymbol{u}_0) \cdot \boldsymbol{e}(\widetilde{\boldsymbol{u}}_\varepsilon) + \Upsilon(\boldsymbol{\sigma}(\widetilde{\boldsymbol{u}}_\varepsilon))) - \Phi(\Upsilon(\boldsymbol{\sigma}(\boldsymbol{u}_0))) - \Phi'(\Upsilon(\boldsymbol{\sigma}(\boldsymbol{u}_0)))(\mathbb{B}\boldsymbol{\sigma}(\boldsymbol{u}_0) \cdot \boldsymbol{e}(\widetilde{\boldsymbol{u}}_\varepsilon) + \xi \mathrm{tr}\boldsymbol{e}(\widetilde{\boldsymbol{u}}_\varepsilon)) \Big] d\boldsymbol{x}. \quad \text{(A.38)}$$

Since $\boldsymbol{u}_\varepsilon$ is the solution of the state equation (A.1), by difference we find that $\widetilde{\boldsymbol{u}}_\varepsilon$ solves:

$$\left\{ \begin{array}{rcll} -\mathrm{div}(\gamma_\varepsilon \boldsymbol{\sigma}(\widetilde{\boldsymbol{u}}_\varepsilon)) & = & 0 & \text{in} \quad B_\varepsilon \cup (D \setminus \overline{B_\varepsilon}), \\ [\![\gamma_\varepsilon \boldsymbol{\sigma}(\widetilde{\boldsymbol{u}}_\varepsilon)]\!] \boldsymbol{n} & = & -(\gamma_1 - \gamma_0)\boldsymbol{\sigma}(\boldsymbol{u}_0)\boldsymbol{n} & \text{on} \quad \partial B_\varepsilon, \\ \widetilde{\boldsymbol{u}}_\varepsilon & = & 0 & \text{on} \quad \Gamma_D, \\ \boldsymbol{\sigma}(\widetilde{\boldsymbol{u}}_\varepsilon)\boldsymbol{n} & = & 0 & \text{on} \quad \Gamma_N \cup \Gamma_0. \end{array} \right. \quad \text{(A.39)}$$

By setting now $\boldsymbol{S} = \boldsymbol{\sigma}(\boldsymbol{u}_0(\widehat{\boldsymbol{x}}))$, we approximate $\widetilde{\boldsymbol{u}}_\varepsilon$ by $\boldsymbol{h}_\varepsilon^S$ – the solution of the auxiliary problem (A.24). Then, we have

$$V_{J1}(\varepsilon) = \int_{\widetilde{D}} \gamma_\varepsilon \Big[\Phi(\Upsilon(\boldsymbol{\sigma}(\boldsymbol{u}_0)) + \mathbb{B}\boldsymbol{\sigma}(\boldsymbol{u}_0) \cdot \boldsymbol{e}(\boldsymbol{h}_\varepsilon^S) + \Upsilon(\boldsymbol{\sigma}(\boldsymbol{h}_\varepsilon^S))) - \Phi(\Upsilon(\boldsymbol{\sigma}(\boldsymbol{u}_0))) - \Phi'(\Upsilon(\boldsymbol{\sigma}(\boldsymbol{u}_0)))(\mathbb{B}\boldsymbol{\sigma}(\boldsymbol{u}_0) \cdot \boldsymbol{e}(\boldsymbol{h}_\varepsilon^S) + \xi \mathrm{tr}\boldsymbol{e}(\boldsymbol{h}_\varepsilon^S)) \Big] d\boldsymbol{x} + \mathcal{E}_4(\varepsilon). \quad \text{(A.40)}$$

If $\widehat{\boldsymbol{x}} \in D \setminus \overline{\widetilde{D}}$, by using a Taylor expansion of Φ and the estimate $|\boldsymbol{\sigma}(\boldsymbol{h}_\varepsilon^S)(\boldsymbol{x})| = o(\varepsilon^2)$ which holds uniformly with respect to $\boldsymbol{x}$ a fixed distance away from $\widehat{\boldsymbol{x}}$, we can easily establish that $V_{J1}(\varepsilon) = o(\varepsilon^2)$. Thus we assume that $\widehat{\boldsymbol{x}} \in \widetilde{D}$ (the special case where $\widehat{\boldsymbol{x}} \in \partial\widetilde{D}$ is not treated). In view of the decay of $\boldsymbol{\sigma}(\boldsymbol{h}_\varepsilon^S)$ at infinity and the regularity of $\boldsymbol{u}_0$ near $\widehat{\boldsymbol{x}}$, we write

$$V_{J1}(\varepsilon) = \int_{\Re^2} \gamma_\varepsilon^* \Big[\Phi(\Upsilon(\boldsymbol{\sigma}(\boldsymbol{u}_0))(\widehat{\boldsymbol{x}}) + \mathbb{B}\boldsymbol{\sigma}(\boldsymbol{u}_0)(\widehat{\boldsymbol{x}}) \cdot \boldsymbol{e}(\boldsymbol{h}_\varepsilon^S) + \Upsilon(\boldsymbol{\sigma}(\boldsymbol{h}_\varepsilon^S))) - \Phi(\Upsilon(\boldsymbol{\sigma}(\boldsymbol{u}_0))(\widehat{\boldsymbol{x}})) - \Phi'(\Upsilon(\boldsymbol{\sigma}(\boldsymbol{u}_0))(\widehat{\boldsymbol{x}}))(\mathbb{B}\boldsymbol{\sigma}(\boldsymbol{u}_0)(\widehat{\boldsymbol{x}}) \cdot \boldsymbol{e}(\boldsymbol{h}_\varepsilon^S) + \xi \mathrm{tr}\boldsymbol{e}(\boldsymbol{h}_\varepsilon^S)) \Big] d\boldsymbol{x} + \mathcal{E}_4(\varepsilon) + \mathcal{E}_5(\varepsilon), \quad \text{(A.41)}$$

with $\gamma_\varepsilon^*(\boldsymbol{x}) = \gamma_1(\widehat{\boldsymbol{x}})$ if $\boldsymbol{x} \in B_\varepsilon$ and $\gamma_\varepsilon^*(\boldsymbol{x}) = \gamma_0(\widehat{\boldsymbol{x}})$ otherwise. The above expression can be rewritten as

$$V_{J1}(\varepsilon) = \int_{\Re^2} \gamma_\varepsilon^* \Big[\Phi(\tfrac{1}{2}\widetilde{\mathbb{B}}\boldsymbol{S}\cdot\boldsymbol{S} + 2\eta\overline{\sigma}\mathrm{tr}\boldsymbol{S} + \widetilde{\mathbb{B}}\boldsymbol{S}\cdot\boldsymbol{\sigma}(\boldsymbol{h}_\varepsilon^S) + 2\eta\overline{\sigma}\mathrm{tr}\boldsymbol{\sigma}(\boldsymbol{h}_\varepsilon^S) + \tfrac{1}{2}\widetilde{\mathbb{B}}\boldsymbol{\sigma}(\boldsymbol{h}_\varepsilon^S)\cdot\boldsymbol{\sigma}(\boldsymbol{h}_\varepsilon^S)) -$$
$$\Phi(\tfrac{1}{2}\widetilde{\mathbb{B}}\boldsymbol{S}\cdot\boldsymbol{S} + 2\eta\overline{\sigma}\mathrm{tr}\boldsymbol{S}) - \Phi'(\tfrac{1}{2}\widetilde{\mathbb{B}}\boldsymbol{S}\cdot\boldsymbol{S} + 2\eta\overline{\sigma}\mathrm{tr}\boldsymbol{S})(\widetilde{\mathbb{B}}\boldsymbol{S}\cdot\boldsymbol{\sigma}(\boldsymbol{h}_\varepsilon^S) + 2\eta\overline{\sigma}\mathrm{tr}\boldsymbol{\sigma}(\boldsymbol{h}_\varepsilon^S)) \Big] d\boldsymbol{x} + \mathcal{E}_4(\varepsilon) + \mathcal{E}_5(\varepsilon). \tag{A.42}$$

We shall denote $V_{J11}(\varepsilon)$ and $V_{J12}(\varepsilon)$ the parts of the above integral computed over B_ε and $\Re^2 \setminus \overline{B_\varepsilon}$, respectively. By using the expressions (A.28)-(A.30), we find

$$V_{J11}(\varepsilon) = \pi\varepsilon^2\gamma_1(\widehat{\boldsymbol{x}}) \Big[\Phi(\tfrac{1}{2}\widetilde{\mathbb{B}}\boldsymbol{S}\cdot\boldsymbol{S} + 2\eta\overline{\sigma}\mathrm{tr}\boldsymbol{S} - \rho(\widetilde{\mathbb{B}}\boldsymbol{x}\cdot\mathbb{T}\boldsymbol{S} + 2\eta\overline{\sigma}\mathrm{tr}(\mathbb{T}\boldsymbol{S})) + \rho^2\tfrac{1}{2}\widetilde{\mathbb{B}}\mathbb{T}\boldsymbol{S}\cdot\mathbb{T}\boldsymbol{S}) -$$
$$\Phi(\tfrac{1}{2}\widetilde{\mathbb{B}}\boldsymbol{S}\cdot\boldsymbol{S} + 2\eta\overline{\sigma}\mathrm{tr}\boldsymbol{S}) + \rho\Phi'(\frac{1}{2}\widetilde{\mathbb{B}}\boldsymbol{S}\cdot\boldsymbol{S} + 2\eta\overline{\sigma}\mathrm{tr}\boldsymbol{S})(\widetilde{\mathbb{B}}\boldsymbol{S}\cdot\mathbb{T}\boldsymbol{S} + 2\eta\overline{\sigma}\mathrm{tr}(\mathbb{T}\boldsymbol{S})) \Big]. \tag{A.43}$$

Next, we define the following function:

$$\boldsymbol{S}_\rho^S(\boldsymbol{x}) := \boldsymbol{\sigma}(\boldsymbol{h}_\varepsilon^S)(\varepsilon\boldsymbol{x}), \tag{A.44}$$

which is independent of ε. Then, a change of variable of the form $\boldsymbol{y} = \varepsilon^{-1}\boldsymbol{x}$ yields

$$V_{J12}(\varepsilon) = \varepsilon^2 \int_{\Re^2\setminus\overline{B}} \gamma_0(\widehat{\boldsymbol{x}}) \Big[\Phi(\tfrac{1}{2}\widetilde{\mathbb{B}}\boldsymbol{S}\cdot\boldsymbol{S} + 2\eta\overline{\sigma}\mathrm{tr}\boldsymbol{S} + \widetilde{\mathbb{B}}\boldsymbol{S}\cdot\boldsymbol{S}_\rho^S + 2\eta\overline{\sigma}\mathrm{tr}\boldsymbol{S}_\rho^S + \tfrac{1}{2}\widetilde{\mathbb{B}}\boldsymbol{S}_\rho^S\cdot\boldsymbol{S}_\rho^S) -$$
$$\Phi(\tfrac{1}{2}\widetilde{\mathbb{B}}\boldsymbol{S}\cdot\boldsymbol{S} + 2\eta\overline{\sigma}\mathrm{tr}\boldsymbol{S}) - \Phi'(\tfrac{1}{2}\widetilde{\mathbb{B}}\boldsymbol{S}\cdot\boldsymbol{S} + 2\eta\overline{\sigma}\mathrm{tr}\boldsymbol{S})(\widetilde{\mathbb{B}}\boldsymbol{S}\cdot\boldsymbol{S}_\rho^S + 2\eta\overline{\sigma}\mathrm{tr}\boldsymbol{S}_\rho^S) \Big] d\boldsymbol{y}. \tag{A.45}$$

Next, we set

$$\Psi_\rho(\boldsymbol{S}) := \int_{\Re^2\setminus\overline{B}} \Big[\Phi(\tfrac{1}{2}\widetilde{\mathbb{B}}\boldsymbol{S}\cdot\boldsymbol{S} + 2\eta\overline{\sigma}\mathrm{tr}\boldsymbol{S} + \widetilde{\mathbb{B}}\boldsymbol{S}\cdot\boldsymbol{S}_\rho^S + \tfrac{1}{2}\widetilde{\mathbb{B}}\boldsymbol{S}_\rho^S\cdot\boldsymbol{S}_\rho^S + 2\eta\overline{\sigma}\mathrm{tr}\boldsymbol{S}_\rho^S) -$$
$$\Phi(\tfrac{1}{2}\widetilde{\mathbb{B}}\boldsymbol{S}\cdot\boldsymbol{S} + 2\eta\overline{\sigma}\mathrm{tr}\boldsymbol{S})) - \Phi'(\tfrac{1}{2}\widetilde{\mathbb{B}}\boldsymbol{S}\cdot\boldsymbol{S} + 2\eta\overline{\sigma}\mathrm{tr}\boldsymbol{S})(\widetilde{\mathbb{B}}\boldsymbol{S}\cdot\boldsymbol{S}_\rho^S + \tfrac{1}{2}\widetilde{\mathbb{B}}\boldsymbol{S}_\rho^S\cdot\boldsymbol{S}_\rho^S + 2\eta\overline{\sigma}\mathrm{tr}\boldsymbol{S}_\rho^S) \Big] d\boldsymbol{y}. \tag{A.46}$$

The extra term $\frac{1}{2}\widetilde{\mathbb{B}}\boldsymbol{S}_\rho^S\cdot\boldsymbol{S}_\rho^S$ has been added so that $\Psi_\rho(\boldsymbol{S})$ vanishes whenever Φ is linear. Thus we have

$$V_{J12}(\varepsilon)=\varepsilon^2\gamma_0(\widehat{\boldsymbol{x}})\left[\Psi_\rho(\boldsymbol{S})+\tfrac{1}{2}\Phi'(\tfrac{1}{2}\widetilde{\mathbb{B}}\boldsymbol{S}\cdot\boldsymbol{S}+2\eta\overline{\sigma}\mathrm{tr}\boldsymbol{S})\int_{\Re^2\setminus\overline{B}}\widetilde{\mathbb{B}}\boldsymbol{S}_\rho^S\cdot\boldsymbol{S}_\rho^S d\boldsymbol{y}\right]. \quad \text{(A.47)}$$

By using the expressions (A.25)–(A.27), a symbolic calculation of the above integral gives

$$V_{J12}(\varepsilon)=\varepsilon^2\gamma_0(\widehat{\boldsymbol{x}})\left[\Psi_\rho(\boldsymbol{S})+\tfrac{1}{4}\pi\rho^2k_1(\boldsymbol{u}_0)(\widehat{\boldsymbol{x}})\left((5-8\eta^2)(2\boldsymbol{S}\cdot\boldsymbol{S}-\mathrm{tr}^2\boldsymbol{S})+3\left(\frac{1+b\gamma}{1+a\gamma}\right)^2\mathrm{tr}^2\boldsymbol{S}\right)\right]. \quad \text{(A.48)}$$

Further, after a change of variable and rearrangements, $\Psi_\rho(\boldsymbol{S})$ reduces to (49), with $\boldsymbol{S}=\boldsymbol{\sigma}(\boldsymbol{u}_0(\widehat{\boldsymbol{x}}))$. Finally, we obtain:

$$\begin{aligned}VJ_1(\varepsilon)=\pi\gamma_1(\widehat{\boldsymbol{x}})\Big[&\Phi(\tfrac{1}{2}\widetilde{\mathbb{B}}\boldsymbol{S}\cdot\boldsymbol{S}+2\eta\overline{\sigma}\mathrm{tr}\boldsymbol{S}-\rho(\widetilde{\mathbb{B}}\boldsymbol{S}\cdot\mathbb{T}\boldsymbol{S}+2\eta\overline{\sigma}\mathrm{tr}(\mathbb{T}\boldsymbol{S}))+\rho^2\tfrac{1}{2}\widetilde{\mathbb{B}}\mathbb{T}\boldsymbol{S}\cdot\mathbb{T}\boldsymbol{S})-\\&\Phi(\tfrac{1}{2}\widetilde{\mathbb{B}}\boldsymbol{S}\cdot\boldsymbol{S}+2\eta\overline{\sigma}\mathrm{tr}\boldsymbol{S})+\rho\Phi'(\tfrac{1}{2}\widetilde{\mathbb{B}}\boldsymbol{S}\cdot\boldsymbol{S}+2\eta\overline{\sigma}\mathrm{tr}\boldsymbol{S})(\widetilde{\mathbb{B}}\boldsymbol{S}\cdot\mathbb{T}\boldsymbol{S}+2\eta\overline{\sigma}\mathrm{tr}(\mathbb{T}\boldsymbol{S}))\Big]+\\&\gamma_0(\widehat{\boldsymbol{x}})\left[\Psi_\rho(\boldsymbol{S})+\tfrac{1}{4}\pi\rho^2k_1(\boldsymbol{u}_0)(\widehat{\boldsymbol{x}})\left((5-8\eta^2)(2\boldsymbol{S}\cdot\boldsymbol{S}-\mathrm{tr}^2\boldsymbol{S})+3\left(\frac{1+b\gamma}{1+a\gamma}\right)^2\mathrm{tr}^2\boldsymbol{S}\right)\right]+\\&\mathcal{E}_4(\varepsilon)+\mathcal{E}_5(\varepsilon). \quad \text{(A.49)}\end{aligned}$$

Appendix A.4. Partial variation of the penalty functional with respect to the domain

The last term is easily treated as follows:

$$\begin{aligned}VJ_2(\varepsilon) &:= J_\varepsilon(\boldsymbol{u}_0)-J_0(\boldsymbol{u}_0)\\&= \int_{B_\varepsilon\cap\widetilde{D}}(\gamma_1-\gamma_0)\Phi(\Upsilon(\boldsymbol{\sigma}(\boldsymbol{u}_0)))d\boldsymbol{x}\\&= \pi\varepsilon^2\chi_{\widetilde{D}}(\widehat{x})(\gamma_1-\gamma_0)(\widehat{\boldsymbol{x}})\Phi(\Upsilon(\boldsymbol{\sigma}(\boldsymbol{u}_0))(\widehat{\boldsymbol{x}}))+\mathcal{E}_6(\varepsilon)\\&= \pi\varepsilon^2\chi_{\widetilde{D}}(\widehat{\boldsymbol{x}})(\gamma_1-\gamma_0)(\widehat{\boldsymbol{x}})\Phi(\tfrac{1}{2}\widetilde{\mathbb{B}}\boldsymbol{S}\cdot\boldsymbol{S}+2\eta\overline{\sigma}\mathrm{tr}\boldsymbol{S})+\mathcal{E}_6(\varepsilon). \quad \text{(A.50)}\end{aligned}$$

Appendix A.5. Topological derivative

Analogously to the derivation presented in [6] which dealt with the Laplace equation, with the regularity resulting from assumptions 1 and 2 surrounding

equation (A.17) we can prove that the remainders $\mathcal{E}_1(\varepsilon), \cdots, \mathcal{E}_6(\varepsilon)$ identified in the above analysis behave as $o(\varepsilon^2)$. Hence, after the summation of the different terms according to Proposition 5 followed by a few simplifications, we finally arrive at the following exact formula for the topological asymptotic expansion of the penalty functional:

$$J_\varepsilon(u_\varepsilon) - J_0(u_0) = \varepsilon^2 D_T J_\Omega + o(\varepsilon^2), \tag{A.51}$$

with the topological derivative $D_T J_\Omega$ given by (44).

[1] G. Allaire. *Conception optimale de structures*. Volume 58 of Mathématiques et applications. Springer-Verlag, Berlin, 2007.

[2] G. Allaire, F. Jouve, & H. Maillot. Topology optimization for minimum stress design with the homogenization method. *Structural and Multidisciplinary Optimization*, 28(2-3):87–98, 2004.

[3] G. Allaire & F. Jouve. Minimum stress optimal design with the level-set method. *Engineering Analysis with Boundary Elements. Special issue*, 32(11):909–918, 2008.

[4] S. Amstutz. Sensitivity analysis with respect to a local perturbation of the material property. *Asymptotic Analysis*, 49(1-2):87–108, 2006.

[5] S. Amstutz & H. Andrä. A new algorithm for topology optimization using a level-set method. *Journal of Computational Physics*, 216(2):573–588, 2006.

[6] S. Amstutz. A penalty method for topology optimization subject to a pointwise state constraint. *ESAIM: Control, Optimisation and Calculus of Variations*, 16(03):523–544, 2010.

[7] S. Amstutz, S.M. Giusti, A.A. Novotny & E.A de Souza Neto. Topological derivative for multi-scale linear elasticity models applied to the synthesis of microstructures. *International Journal for Numerical Methods in Engineering*, 84:733–756, 2010.

[8] S. Amstutz & A.A. Novotny. Topological optimization of structures subject to von Mises stress constraints. *Structural and Multidisciplinary Optimization*, 41:407–420, 2010.

[9] M. P. Bendsøe & N. Kikuchi. Generating optimal topologies in structural design using a homogenization method. *Computer Methods in Applied Mechanics and Engineering*, 71(2):197–224, 1988.

[10] M. P. Bendsøe & O. Sigmund. *Topology optimization. Theory, methods and applications*. Springer-Verlag, Berlin, 2003.

[11] M. Burger & R. Stainko. Phase-field relaxation of topology optimization with local stress constraints. *SIAM Journal on Control and Optimization*, 45(4):1447–1466, 2006.

[12] J. Céa, S. Garreau, Ph. Guillaume & M. Masmoudi. The shape and Topological Optimizations Connection. *Computer Methods in Applied Mechanics and Engineering*, 188(4):713–726, 2000.

[13] E.A. de Souza Neto, D. Perić & D.R.J. Owen. *Computational Methods for Plasticity. Theory and Applications*. Wiley, Chichester, 2008.

[14] P. Duysinx & M. P. Bendsøe. Topology optimization of continuum structures with local stress constraints. *International Journal for Numerical Methods in Engineering*, (43):1453–1478, 1998.

[15] D.C. Drucker & W. Prager. Soil Mechanics and Plasticity Analysis of Limit Design. *Quarterly Journal of Applied Mathematics*, 10:157–162, 1952.

[16] H.A. Eschenauer & N. Olhoff. Topology Optimization of Continuum Structures: A Review. *Applied Mechanics Review*, 54:331–390, 2001.

[17] H.A. Eschenauer, V.V. Kobelev & A. Schumacher. Bubble Method for Topology and Shape Optimization of Structures. *Structural Optimization*, 8:42–51, 1994.

[18] E.A. Fancello. Topology optimization for minimum mass design considering local failure constraints and contact boundary conditions. *Structural and Multidisciplinary Optimization*, 32(3):229–240, 2006.

[19] Genesis® Structural Analysis and Optimization Software. Vanderplaats Research & Development, Inc. Web page http://www.vrand.com/Genesis.html.

[20] S.M. Giusti, A.A. Novotny & C. Padra. Topological sensitivity analysis of inclusion in two-dimensional linear elasticity. *Engineering Analysis with Boundary Elements*, 32(11):926–935, 2008.

[21] D. Knees, A.-M. Sändig. *Regularity of elastic fields in composites*. Multifield problems in solid and fluid mechanics, Lecture Notes on Applied Computational Mechanics, 28:331–360, Springer, Berlin, 2006.

[22] C. Le, J. Norato, T. Bruns, C. Ha & D. Tortorelli. Stress-based topology optimization for continua. *Structural and Multidisciplinary Optimization*, 41:605–620, 2010.

[23] R. W. Little. *Elasticity*. Prentice-Hall, New Jersey, 1973.

[24] S. A. Nazarov & J. Sokolowski. Asymptotic analysis of shape functionals. *Journal de Mathematiques Pures et Appliquees*, 82(2):125–196, 2003.

[25] J.A. Norato, M.P. Bendsøe, R.B. Haber & D. Tortorelli. A topological derivative method for topology optimization. *Structural and Multidisciplinary Optimization*, 33(4-5):375–386, 2007.

[26] A.A. Novotny, R.A. Feijóo, C. Padra & E. Taroco. Topological sensitivity analysis. *Computer Methods in Applied Mechanics and Engineering*, 192(7-8):803–829, 2003.

[27] A.A. Novotny, R.A. Feijóo, E. Taroco & C. Padra. Topological sensitivity analysis for three-diensional elasticity problem. *Computer Methods in Applied Mechanics and Engineering*, 196(41-44):4354–4364, 2007.

[28] Altair® OptiStruct®. Altair Engineering, Inc. Web page http://www.altairhyperworks.com.

[29] J.T. Pereira, E.A. Fancello & C.S. Barcellos. Topology optimization of continuum structures with material failure constraints. *Structural and Multidisciplinary Optimization*, 26(1-2):50–66, 2004.

[30] J. Rocha de Faria & A.A. Novotny. On the second order topological asymptotic expansion. *Structural and Multidisciplinary Optimization*, 39(6):50–66, 2009.

[31] J. Sokolowski & A. Zochowski. On the Topological Derivatives in Shape Optmization. *SIAM Journal on Control and Optimization*, 37(4):1251–1272, 1999.